8-2022

Evaluation of Carbon Isotopic Chemostratigraphy of the Cedar Mountain Formation of Utah

Clayton Forster
University of Arkansas, Fayetteville

Evaluation of Carbon Isotopic Chemostratigraphy of the Cedar Mountain Formation of Utah

A thesis submitted in partial fulfillment
of the requirements for the degree of
Master of Science in Geology

by

Clayton Forster
Utah Valley University
Bachelor of Science in Geology, 2019

August 2022
University of Arkansas

This thesis is approved for recommendation to the Graduate Council.

_____
Celina Suarez, Ph.D.
Thesis Director

_____
Glenn Sharman, Ph.D.
Committee Member

_____
Phillip Hays, Ph.D.
Committee Member

Abstract:

The Lower Cretaceous rocks of Utah preserve the origin of a multitude of dinosaur taxa, spread of angiosperms on the North American continent, and evolution of marsupial and eutherian mammals. However, the timing of deposition of these rocks is not well understood and must be determined to understand climatic controls on these biological events. Estimates of the age of the Cedar Mountain Formation and its constituent members range from Late Jurassic to early Late Cretaceous. Understanding the timing of deposition of the Cedar Mountain Formation is critical to dinosaurian and associated taxa studies as well as paleoclimate reconstructions from within the Cedar Mountain Formation. It is also critical to understanding the present climate as the earliest Cretaceous is an example of a "coolhouse" world transitioning to a "warmhouse" world similar to our current world transition and future climate.

Stable carbon isotope chemostratigraphy of two outcrops of the Yellow Cat Member and an exposure of the Mussentuchit Member at Moore Cutoff Road and east of Green River, Utah are reported on here. This study identifies two major positive carbon isotope excursions with one occurring in the Yellow Cat Member with a magnitude of ~+4‰ and one in the Mussentuchit Member with a magnitude of ~+3‰. We interpret that the Yellow Cat Member records a terrestrial response to the oceanic anoxic event known as the Weissert Event, based on comparison with similar C-isotope chemostratigraphic curves from other oceanic and terrestrial records. This oceanic C-isotope record is associated with the coeval Paraná-Etendeka large igneous province emplacement. The Mussentuchit Member, like the Yellow Cat Member, includes a terrestrial response to an oceanic anoxic event, in this case, the Mid-Cenomanian Event. These results imply the potential existence of terrestrial evidence of other anoxic events OAE 1a, OAE 1b (i.e., "Leenhardt" and "Paquier" events), Jassines (OAE 1c), and OAE 1d

within the Ruby Ranch Member, the age of the Yellow Cat Member spans from the Berriasian to Aptian, and the Mussentuchit Member chemostratigraphy aligns with ages from detrital zircon analyses pointing to deposition occurring within the Cenomanian.

Acknowledgements

Completing a degree through a global pandemic has been one of the weirdest experiences of my life, but the time I spent at the University of Arkansas has been incredibly intellectually fulfilling. First, I would like to thank my advisor, Dr. Celina Suarez, who gave me her guidance, confidence, and thoroughness in the scientific process. She taught me a significant amount about science, geochemistry, and the Cretaceous of North America which I intend on spending much more time contemplating with her in the future. My thesis co-advisor, Dr. Glenn Sharman was instrumental in the completion of this thesis for everything from sample collection to the edits on this thesis along with Dr. Phillip Hays, who provided me a solid background in stable isotope geochemistry.

None of this would have been possible without the amazing mass spectrometry work of Lindsey Conaway and Erik Pollock within the University of Arkansas Stable Isotope Laboratory who were there for every sample I ran. I look forward to sending many more samples there and continually working with them.

Lastly, I would like to thank my family, my Mom, Dad, and my siblings Glen, Lindsay, and Garret for their undying support and help to set me down this path and tolerating my ever-growing rock collection.

Table of Contents

List of Figures:

Chapter 1: Introduction

C-Isotope Chemostratigraphy and the Carbon Cycle

Carbon has two stable isotopes, carbon-12 and carbon-13. Within the Solar System, the ratio between the two is around 0.01 (White, 2014). This difference in the number of neutrons allows for fractionation or discrimination of the different masses based on the weight differences or also called "mass dependent fractionation" (White, 2014). This small difference in weight can change the ratio of light to heavy isotopes within a substance. The way this is quantified is by taking the ratio of the number of heavy to light isotopes in a sample and comparing it to that of a defined standard, for example, carbon isotopes are frequently compared to the standard Vienna PeeDee Belemnite as seen in Equation 1. This equation is equal to a 'delta' value that can be compared between samples and standards.

Equation 1

$$\delta^{13}C=\left[\frac{(^{13}C/^{12}C)_{sample}-(^{13}C/^{12}C)_{VPDB}}{(^{13}C/^{12}C)_{VPDB}}\right] \times 1000$$

Fractionation by mass leads to two different states of fractionating, one when two bodies of the element of study is at equilibrium (for example, oxygen in the water in the atmosphere and oxygen in the water in the ocean with no net change between the two) and one when there is a unidirectional path for the element so that there is a net change in the concentration in the source and in the sink. An example of the second unidirectional fractionation or 'kinetic' fractionation for carbon is a process like photosynthesis in plants and algae (White, 2014). This is the process that will be focused on within this study.

Photosynthesis is simply the process that a plant uses to extract carbon from the atmosphere to produce sugars and cellulose, but the process from sunlight to sugar can be classed into two different pathways: C_3 and C_4. C_4 plants did not become dominant until Miocene time and are climatically restricted. Thus, for the purposes of this study the C_4 photosynthesis pathway will be ignored (Arens et al., 2000). The first step within the C_3 pathway is the diffusion of CO_2 into the stomata of the plant. The simple difference of weight between $^{13}CO_2$ and $^{12}CO_2$ can theoretically produce a per-mil (‰) difference of 4.4‰ (White, 2014). So, the CO_2 that makes it into the plant will show a value of approximately -4.4‰ relative to atmosphere.

After the initial diffusion into the plant the CO_2 is split and goes through the Calvin cycle which produces sucrose, starches, shikimic acid, and isoprenoids which are used in other processes, stored, or expelled (Raines, 2003). The Calvin cycle produces a kinetic fractionation of about -29.4‰ within C_3 plants and around -20‰ in photosynthetic bacteria due to some slightly different mechanisms (White, 2014). In plants, there is a total fractionation potential of ~-34‰ but due to constraints on the CO_2 concentration in the atmosphere and the amount of CO_2 required by the plant the full value fractionation is rarely reached with a typical total fractionation of between -20 to -30‰ (White, 2014). This is verified empirically by analysis of various types of fossilized plant and other associated organic matter from the last 450 Ma yr where the average $\delta^{13}C$ of all fossilized organic matter was -24.6 ± 1.7‰ (Nordt et al., 2016).

For this study, analysis of fossilized organic matter is the chosen method for chemostratigraphic correlation. This is a viable method of chronostratigraphic correlation as the isotopic composition of the atmosphere changes over time. These changes are referred to as ‘excursions’ and are recorded in the isotopic composition of organic matter (which is preserved in ancient sedimentary rocks) throughout time. While there are studies that show pCO_2 in the

atmosphere has the potential to shift the average $\delta^{13}C$ of organic matter, secular forces on the atmosphere override this effect to produce the excursions used for correlation (Nordt et al., 2016). These excursions can be driven by increases in rates of volcanism, subduction, and/or weathering in addition to biosphere and soil drawdown. Volcanic eruptions will temporarily increase the pCO_2 as well as enrich the atmosphere with ^{13}C producing positive carbon isotope excursions (PCIEs). Weathering, sedimentation, and burial of organic matter will decrease the pCO_2 in the atmosphere and decrease the average $\delta^{13}C$ of the atmosphere which produces negative carbon isotope excursions (NCIEs). Frequently PCIEs and NCIEs are coupled representing a negative feedback loop between volcanism and organic carbon burial. Examples of PCIEs and NCIEs can be found within Cretaceous-age sedimentary rock.

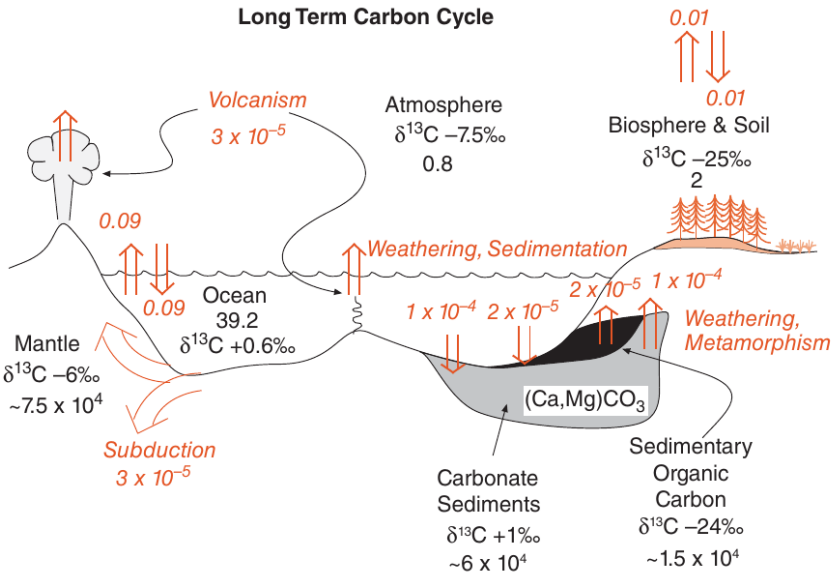

Figure 1: The long-term carbon cycle prior to the Industrial Revolution. The black numbers represent reservoirs of carbon with amounts in 10^{18} grams. The fluxes between reservoirs are shown in orange arrows and italics in units of 10^{18} g/yr. The uncertainties on the masses and fluxes are large so these are just general estimates. Also shown are estimates of the carbon isotopic composition of each reservoir. Note that the sedimentary organic carbon value is nearly identical to the biosphere and soil value representing the link to photosynthetic organic matter input. Modified from White (2014, pg. 352).

Cretaceous Climate and Ocean Anoxic Events: Effects on $\delta^{13}C_{organic}$ in the Cretaceous

The Cretaceous is thought to be a time of overall global warmth. However, the climatic history of this ~79-million-year time period suggests several instances of global cooling as well (Amiot et al., 2011, 2021). These fluctuations in the Cretaceous climate are often associated with major perturbations to the C-cycle, resulting in both warming and cooling, as well as related global oceanic anoxia (ocean anoxic events, OAE). These fluctuations in the global carbon cycle have a carbon isotopic signature, manifested as changes in $\delta^{13}C$, that can be observed in the bulk organic matter and carbonate found within unaltered rocks that date back to this period. A few of these 'coolhouse' and 'warmhouse' periods are associated with eruptions of several large igneous provinces (LIPs) that occur throughout the Cretaceous (Scotese et al., 2021). LIPs sometimes result in widespread ocean anoxia and euxinia (Scotese et al., 2021).

A brief, selective list of the major excursions during the Early Cretaceous and early Late Cretaceous is as follows: 1) a positive carbon isotope excursion (PCIE) associated with the emplacement (136 Ma-129 Ma) of the Paraná-Etendeka LIP. Rift volcanos that formed as a consequence of the rifting of South America and Africa resulted in the Paraná-Etendeka LIP (Schettino and Scotese, 2005; Seton et al., 2012). These eruptions sent immense amounts of carbon dioxide into the atmosphere from the interior as part of an eruption of flood basalts covering an area that would become part of the countries Uruguay, Brazil, and Namibia (Martinez et al., 2015 and references therein). Chronologically coinciding events such as the marine Weissert Event in the Valanginian (Erba et al., 2004) and methane hydrate dissociation events (Jahren et al., 2001) also contributed to the carbon isotopic record around the time of the Paraná-Etendeka LIP eruption. The ocean anoxia described as the Weissert Event is hypothesized to have been driven by nutrification of the oceans by the outgassing of CO_2 from

the Paraná-Etendeka LIP (Erba et al., 2004; Weissert and Erba, 2004; Grocke et al., 2005; Gréselle et al., 2011; Martinez et al., 2015; Cavalheiro et al., 2021). 2) A brief, relatively minor excursion called the Faraoni Event occurs in the latest Hauterivian but is not well expressed in the $\delta^{13}C$ record (Bodin et al., 2006; Föllmi et al., 2012).

3) In the Pacific Ocean, another LIP, the Ontong-Java LIP, began emplacement at ~126 Ma and concluded ~119 Ma (Neal et al., 1997; Gibson et al., 2006; Tejada et al., 2009; Gomes and Vasconcelos, 2021). This LIP and the associated large volumes of carbon dioxide and other gases released into the atmosphere are thought to be responsible for initiating the Selli Event (OAE 1a) (van Breugel et al., 2007). Examples of the effects of the heightened carbon dioxide include global warming, increased weathering, and higher productivity which all have effects on the carbon isotopic value of the atmosphere as the CO_2 is released and then drawn out of the atmosphere via silicate weathering and increased productivity. The Selli Event has several accompanying NCIEs and PCIEs but is typically composed of a sharp NCIE and subsequent PCIE with the initial portion of the excursions occurring synchronously with the main eruptive phase of the Ontong-Java LIP eruptions (Bodin et al., 2015; Gale et al., 2020 and references therein; Castro et al., 2021).

Within the Albian, there are three ocean anoxic events. Several NCIE excursions which compose '4) OAE 1b' occurred in the Early Albian. This set of NCIEs can be broken down into the Paquier-Urbino, Jacob, Kilian, Leenhardt and l'Arbouysse OAEs (Trabucho-Alexandre et al., 2011; Li et al., 2016; Gale et al., 2020). Unlike some the previous events and some other OAEs, OAE 1b does not include a large positive carbon isotope excursion but rather several NCIEs. The primary influence of this event and subevents is attributed to Milankovich cycles rather than a LIP eruption (Gale et al., 2020). Similar to OAE 1b, 5) OAE 1c in the early-mid

Albian is associated with increased deposition of organic matter accumulating into dark black shales and may be associated with the Jassines Event by other authors (Arthur et al., 1990; Leckie et al., 2002; Gale et al., 2011, 2020). However, there are disagreements as to whether or not black shales and any extinction events are associated with OAE 1c (Erbacher and Thurow, 1997). Later in the late Albian, the third OAE, 6) OAE 1d, occurs (Schlanger and Jenkyns, 1976; Arthur et al., 1990; Erbacher and Thurow, 1997; Scott et al., 2020). This OAE is composed of four PCIEs and are collectively known as OAE 1d or the Albian/Cenomanian Boundary Event (Gale et al., 2020).

In between OAEs 1d and 2, Paul et al., (1994) also discovered a 'double peaked' PCIE that is dated to the mid-Cenomanian and is named as such, "the mid-Cenomanian event (MCE)". This OAE has been recognized in numerous sections despite being a relatively minor excursion, including within hemipelagic sections documented in Tibet (Li et al., 2016), marine sections from the Western Interior Basin in the United States (Joo and Sageman, 2014), and within chalk deposits in the United Kingdom (Herrle et al., 2015).

Lastly, there is a significant PCIE at the Cenomanian-Turonian boundary that is directly correlated to 7) OAE 2, also known as the Bonarelli Event or Thomas Event (Arthur et al., 1990; Jarvis et al., 2006; Eldrett et al., 2014; Joo and Sageman, 2014). OAE 2 is different from the other OAEs as it has a very distinct shape in the C-isotope record associated with it, comprising an initial sharp PCIE, an NCIE, then a PCIE returning the $\delta^{13}C$ to its previous high and plateauing for a brief time period before gradually decreasing after the Turonian boundary (Gale et al., 2020). Marine evidence of OAE 2 is interpreted to be the deposition of "rhythmic organic-rich black shales controlled by orbital forcing" (Gambacorta et al., 2015) and as such multiple layers of black shales are deposited globally (i.e. Schlanger and Jenkyns, 1976; Arthur et al.,

1990; Erbacher and Thurow, 1997; Li et al., 2006; Joo and Sageman, 2014; Herrle et al., 2015). OAE 2 is also correlated to an increase in instances of wildfire in continental environments due to a suppression of the movement of water onto some terrestrial environments (Baker et al., 2020). Terrestrial expression of the atmospheric effects from several of the above events appear to be recorded in the members of the Cedar Mountain Formation (CMF) in east-central Utah and the $\delta^{13}C$ recorded in the organic carbon within its members provide strong constraints on the timing of deposition for the formation.

Brief Geologic Description

In east-central Utah, the CMF was deposited in a terrestrial depositional system during the Early Cretaceous. It consists of several members, typically consisting of the (from stratigraphically lowest to highest) Yellow Cat Member, Poison Strip Member, Ruby Ranch Member, Short Canyon Member, and Mussentuchit Member (Kirkland et al., 2016). Where the Yellow Cat Member pinches out on the western portion of the formation, it interfingers with the Buckhorn Conglomerate and may interfinger with the Poison Strip Member (Kirkland et al., 2016). The Mussentuchit Member is thought to include the Short Canyon Conglomerate Member and may interfinger with the overlying Naturita Formation. Within this work, the focus will be primarily placed on the Yellow Cat, Ruby Ranch, and Mussentuchit members.

The Yellow Cat Member sits unconformably on the Jurassic Morrison Formation. It consists of a mixture of lacustrine, fluvial, and paleosol sediments with inferred debris flow deposits in places (Greenhalgh and Britt, 2007). Much of the sediment is derived from reworking of the underlying Morrison Formation. With these influences, the rock composition varies from reworked red mudstones of the Morrison Formation to dark black lacustrine shales and mudstones. It is typically defined by its drab variegated colors, occurrence of carbonate nodules,

paleosols, and chert pebbles (Greenhalgh and Britt, 2007; Kirkland et al., 2016). Paleontologically, the Yellow Cat Member is important for its abundant dinosaur bones (Greenhalgh and Britt, 2007).

Similarly, the Ruby Ranch Member is known for its abundant dinosaur fauna such as *Tenontosaurus* (Kirkland et al., 2016). Lithologically, the Ruby Ranch Member is similar to the Yellow Cat Member except for its increased abundance of carbonate nodules. The depositional environments of the Ruby Ranch Member include soil mantled overbank deposits, ephemeral ponds, and low-sinuosity rivers that represent semi-arid conditions. One area of special attention is a thick lacustrine section west of the Salt Valley Anticline informally known as "Lake Carpenter" (Kirkland et al., 2016). The Lake Carpenter lacustrine deposit is unique in that is shows signs of aridity (dolomitic layers) as well as well-preserved trackways on its margins (Montgomery, 2014).

A significant change from the Ruby Ranch and Yellow Cat facies is found in the Mussentuchit Member that is underlain by the Short Canyon Member, a relatively thin conglomerate. No fossils, other than recycled Paleozoic invertebrates found within chert cobbles, are found in the Short Canyon Member. This lack in fossil content is in stark contrast to the rich fauna of the Mussentuchit with highly abundant microvertebrate and macrovertebrate assemblages (Kirkland et al., 2016 and references therein) along with well-preserved plant and pollen remains. Unlike the Short Canyon Member that is coarse-grained, the Mussentuchit Member is primarily composed of abundant smectitic clays and mudstones with very few carbonate nodules (Kirkland et al., 2016).

This study will focus on outcrops of these units of the CMF within Emery County, Utah. This study will build on work from numerous authors to construct the first full C-isotope

chemostratigraphic record from the entirety of the CMF (Ludvigson et al., 2010; Kirkland et al., 2016; M. B. Suarez et al., 2017; McColloch, 2019; Joeckel et al., 2020; Tucker et al., 2020; Gottberg, 2022). I find that the time represented within the CMF is extensive and may span from as old as Berriasian (~145 Ma)(Joeckel et al., 2020) to the late Cenomanian (~95 Ma) (Tucker et al., 2020). The age and interpreted depositional rates and unconformities described in this work have significant implications for evolution of North American dinosaurs and the tectonic history of the Sevier foreland basin.

Chapter 2: Chemostratigraphy of the Cedar Mountain Formation

The CMF is an ideal formation to study Early Cretaceous climate. The ages of its oldest and youngest units are unclear, but the CMF may have been deposited from as old as ~140 Ma in the Yellow Cat Member to as young as ~94 Ma in the Mussentuchit Member (Greenhalgh and Britt, 2007; Garrison et al., 2007; Ludvigson et al., 2010; Suarez et al., 2012, 2014; Kirkland et al., 2016; M. B. Suarez et al., 2017; Tucker et al., 2020). Early deposition was terrestrially derived before marine transgression from the north resulted in predominately marine deposits that record the transgression of the Western Interior Seaway (WIS) (Suarez et al., 2012; Joeckel et al., 2020). The continentals units the Yellow Cat Member, Ruby Ranch Member and Mussentuchit Member of the CMF preserve evidence of the past terrestrial environments and extinct ecosystems of the Early Cretaceous and early Late Cretaceous including various species of dinosaurs, crocodilians, mammals, and turtles (Cifelli et al., 1997, 1999; Kirkland et al., 1999; Eberth et al., 2006; Zanno and Makovicky, 2013; Britt et al., 2017).

A brief review of the ages of each member of the CMF is explained below but will focus on the members of the CMF found at the Moore Cutoff Road locality which are (from stratigraphically lowest to highest): the Yellow Cat, Poison Strip, Ruby Ranch, Short Canyon, and Mussentuchit members. With regard to stable isotope chemostratigraphy, the signal of the Weissert Event excursion is hypothesized to be found within the Yellow Cat Member of the CMF (M. B. Suarez et al., 2017; Joeckel et al., 2020). Other dating techniques such as detrital zircon data suggest the maximum depositional age in the Yellow Cat Member to be as young as ~125 Ma (Greenhalgh and Britt, 2007). In contrast, other authors using ostracod biostratigraphy suggest a much older age of ~140-133 Ma. Another study on different section of the Yellow Cat Member indicated a maximum depositional age of $\leq$~136-139 Ma (Hendrix et al., 2015; Joeckel

et al., 2020). In the Ruby Ranch Member, the C10 C-isotope excursion from Bralower et al., (1999) has been documented and may be correlated to the basal portions of OAE 1b (Ludvigson et al., 2010; McColloch, 2019; Gottberg, 2022), supported by radiometric dates of carbonates from the underlying Poison Strip Member at ~119 Ma (which is not present at the Moore Cutoff Road locality) (Ludvigson et al., 2010).

Within the Ruby Ranch Member at Mussentuchit Wash, detrital zircon dates suggest the depositional age for the uppermost Ruby Ranch to be ≤ ~107-112 Ma (Tucker et al., 2020). Deposition of warm, coastal plain terrestrial deposits found within the Mussentuchit Member of the CMF were deposited well after the rifting between South America and Africa, but before the inundation of the North American interior as shown in Figure 2 (Suarez et al., 2012; Joeckel et al., 2020). Recent dates from the Mussentuchit Member found in Mussentuchit Wash by Tucker et al., (2020) suggest an age of deposition for the upper Mussentuchit ≤ ~99-94 Ma with a CA-TIMS date at ≤ 99.68 ± 0.12 Ma for a dinosaur eggshell quarry called Deep Eddy. Also, at Mussentuchit Wash, the lowermost Naturita Formation (overlying the Mussentuchit Member) was dated by CA-TIMS as ≤ 95.64 ± 0.11 Ma (Tucker et al., 2020). While several pieces of evidence thus presented are contradictory or discordant, chemostratigraphic evidence from each member of the CMF provide constraints on the depositional age of the CMF as a whole. To do this, I generated several bulk organic C-isotope records to compare to global C-isotope records.

Methods

Two stratigraphic sections were measured to generate a carbon isotopic chemostratigraphic curve. One section covered the Mussentuchit Member and the Yellow Cat Member of the CMF at a location referred to here as the Moore Cutoff Road locality (Figure 2). This locality is located on the west side of Utah Route 803, south of the towns Moore and Ferron

(lat. 38.93734°, long. -111.07153°; WGS84). The other section spanned the Yellow Cat Member at a location called Jim's Pond (lat. 38.817322°, long. -109.931065°; WGS84) that is located south of I-70, east of the town of Green River, UT, and north of Arches National Park near the Utah- Colorado border (Kirkland et al., 2016; Fig. 2).

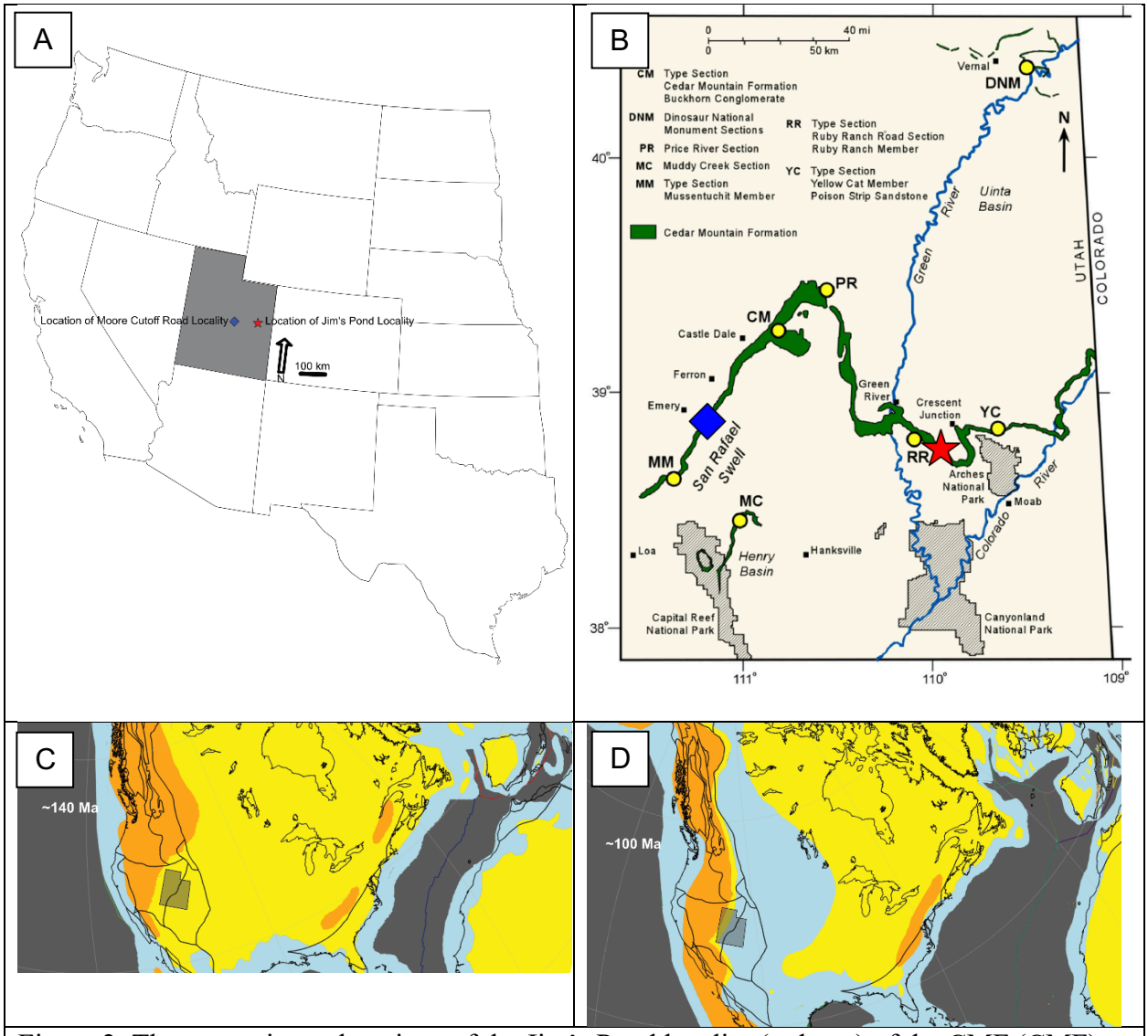

Figure 2: The approximate locations of the Jim's Pond locality (red star) of the CMF (CMF) near Green River, Utah, and of the Moore Cutoff Road Locality (blue diamond) near Moore, Utah. **A,** locations of the sections discussed herein. **B,** a map of the CMF outcrop belt within East-Central Utah (modified from Ludvigson et al. (2015)). **C,** approximate paleo-location of Utah on a paleogeographic map of North America of ~140 Ma modified from Matthews et al., (2016); Cao et al., (2017); and Merdith et al., (2021). Orange represents mountain ranges, yellow represents general landmass, blue represents relatively shallow water and gray represents deeper ocean water. **D,** approximate paleo-location of Utah on a paleogeographic map of North America of ~100 Ma modified from Matthews et al., (2016); Cao et al., (2017); and Merdith et al., (2021). Orange represents mountain ranges, yellow represents general landmass, blue represents relatively shallow water and gray represents deeper ocean water.

Samples were taken every 25 cm from trenched sections in which overburden and colluvium were removed. Lithology and lithologic characteristics such as grain size, color, bedding patterns, sedimentary structures, notable features, such as fossils and foreign rock fragments, were noted for each sample (see appendices A, B, and C). Both sets of samples were analyzed for $\delta^{13}C_{organic}$.

Following the method used by Suarez et al. (2013) to obtain bulk $\delta^{13}C_{organic}$ values, the samples were cleaned of any modern organic material (e.g. roots and burrows). The samples were then crushed into a fine powder by hand using a mortar and pestle. From the crushed sample approximately 1-1.5 g of powder was decarbonated in 30 mL of 3M HCl. The samples were left to react for 2 to 4 hours or until reaction was complete and all carbonate was removed. The samples were then rinsed to neutrality and dried in an oven at 48°C overnight or until the sample was dry. Once dried the samples were then hand crushed into a fine powder again using a mortar and pestle. Each of the newly crushed samples were then weighed out to between 1mg to 15mg. Isotope values were measured on an elemental analyzer (EA) attached to an Thermo Advantage Plus isotope ratio mass spectrometer (IRMS) at the University of Arkansas Stable Isotope Laboratory (UASIL). Each of the samples were packed into 5 x 8 mm tin capsules and pressed closed before incineration. Values are reported in delta notation relative to Vienna Pee Dee Belemnite (VPDB).

Carbon isotopic calibration was determine using an internal standard, Corn Maize (-11.39 ± 0.45‰ 1s, actual = −11.32‰) and White River Trout (-26.62 ±0.08‰, actual=−26.63‰). The percent carbon was calibrated using Black Weeks Sandy Soil (0.84%). Analytical precision and accuracy were monitored via analysis of IAEA - Benzoic Acid (-27.85 ± 0.14‰, actual = -28.81

± 0.04‰) and ANU Sucrose (-10.51 ± 0.26‰, actual=−10.4‰) (actual values are from Suarez et al., (2017)).

Results

Yellow Cat Member

Jim's Pond

A detailed lithostratigraphic description of the section sampled at Jim's Pond can be found in Appendix A. In brief, the unit unconformably lies above the Jurassic Morrison Formation. The base is characterized by alternating pale pink and pale green silty mudstones with occasional floating chert pebbles. The stratigraphy transitions to dark gray organic-rich mudstones which include abundant plant fragments and iron oxide staining with some horizons including abundant ostracods, slickensides, and carbonate nodules indicative of partial subaerial exposure. Interfingered with the mudstones are lithic and quartz sandstones with *Skolithos* trace fossils among other signs of bioturbation. Toward the upper portion of the section, the stratigraphy is dominated by green/gray fine-grained sandstones with carbonate nodules before a return to pale pink and purple mudstones with occasional color changes to green, yellow, or gray.

The $\delta^{13}C_{organic}$ values from the Jim's Pond section range from -29 to -22‰ (Figure 3). The base of the YCM here starts at ~-25‰ representing a pre-excursion value. From the base to ~3.25m, there is an overall NCIE to a minimum of ~-28.5‰ with three oscillations from more negative values to more positive values in an overall increasing $\delta^{13}C$ trend. These oscillations are found within the lacustrine sandstones and mudstones. An increasing trend from the minimum -28.5‰ at 3.25m above the Jurassic Morrison Formation to a maximum of –22.6‰ at 8.25m is situated within the transition from lacustrine sediments to paleosols with pedogenic carbonate nodules. The oscillations continue throughout this part of the section but the 3-point average

increases through this portion of the curve. A characteristic double peak is found within the subaerial paleosols. The double peaks contain the 3-point average maximum value of -21.7‰ and maximum individual sample at -20.4‰ just slightly above 12.25m and comprises the first peak. The NCIE between the two peaks drops to -24.63‰ at ~13.7m. The 3-point average of the second peak is at -23.1‰ at 14.95m. A NCIE pulls the average down to ~ -24.8‰ at 15.60m before returning to a value just below the second peak with a value of ~-23.4‰ for much of the top portion of the section with only a slight deviation towards the top of the section ending the 3-point average at -24.2‰ near 22.5m. The topmost individual sample was taken at 23.70m and has a $\delta^{13}C_{organic}$ of -24.79‰.

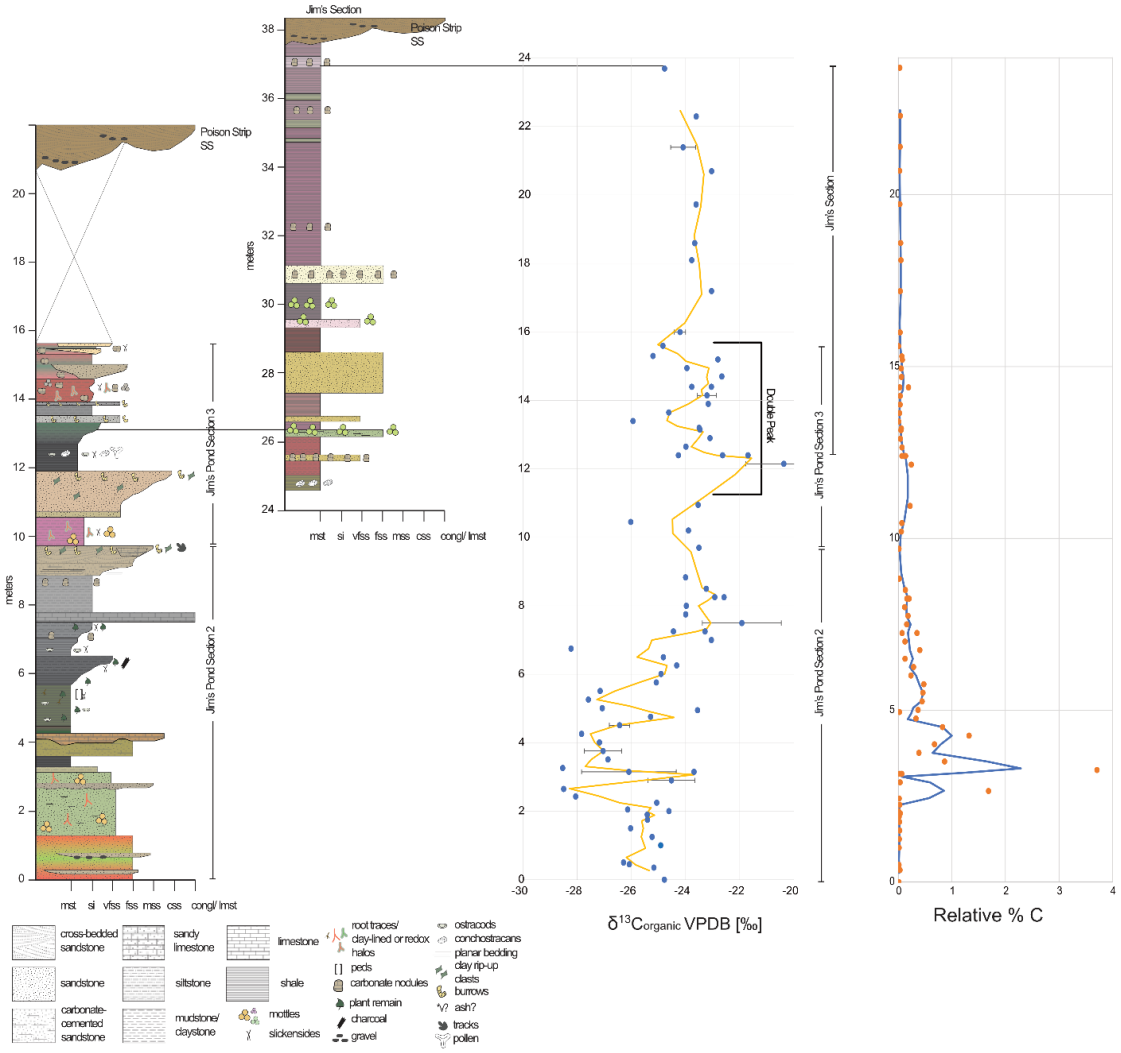

Figure 3: The lithostratigraphy and bulk sedimentary organic carbon stable isotope chemostratigraphy from the Jim's Pond section. Carbon isotope values are compared to VPDB. The lithostratigraphy also includes data from an additional section called Jim's section that includes samples from the covered portion of the original section. The solid black line represents the three-point running average of the individual data points represented by the black-outlined, yellow circles. The abbreviations in the horizontal scale on the lithostratigraphic column represent the following: mst, mudstone; si, siltstone; vfss, very fine sandstone; fss, fine sandstone; mss, medium sandstone; css, course sandstone; congl/lmst, conglomerate/limestone.

Moore Cutoff Road

A detailed lithostratigraphic description of the Yellow Cat and Mussentuchit member sections sampled at Moore Cutoff Road can be found in Appendix B and Appendix C, respectively. A description of the Ruby Ranch Member section at Moore Cutoff Road can be found in Gottberg (2022). Briefly, the Yellow Cat Member unconformably overlies a series of white medium to fine sandstones of the Morrison Formation. The base of the Yellow Cat Member at this location is composed of various shades of purple very-fine sandstones and silty mudstones which commonly have orange, yellow, and/or green mottles. Above the mudstones are red siltstones and sandstones. Within the red siltstones are green, rip-up mud clasts, slickensides, and floating chert gravel. Approximately 7 to 8m into the section a very hard multicolored silcrete occurs. The silcrete is interbedded with the red-purple mudstones above it. Within the overlying mudstones are frequent, large, silicified root casts that are laterally extensive. Above the silcrete-mudstone layers are additional red-purple siltstones with gravel, green rip-up mud clasts, green mottles and occasional to rare carbonate nodules.

The values of the $\delta^{13}C_{organic}$ within the Moore Cutoff Road section show a similar pattern to that in the Jim's Pond section but with much smaller amplitude oscillations. The base of the section here starts with a pre-excursion value of ~ -26‰ found within the fine sandstones with a NCIE at the base of the silcrete layer ~ 6.5m up from the Morrison Formation contact (Figure 4). A similar double peak seen in the Jim's Pond section occurs in this section as well. The initial PCIE reaches a maximum of -22.88‰ at 9.7m within the grey-pink fine mottled-sandstones (first of the doublet) and is followed by a trough that reaches a minimum of ~-25‰ at 10.27 m. The initial PCIE is followed by the second peak of the doublet and reaches a maximum value of -23.8‰ at 11.77m. The second peak coincides with a return to fine sandstones from the lacustrine

muddy siltstones within the interpeak minimum C-isotopes value. The C-isotopes values then decrease consistently from this point throughout the remainder of the sampled section and coincide with a lithologic change to red silty mudstones.

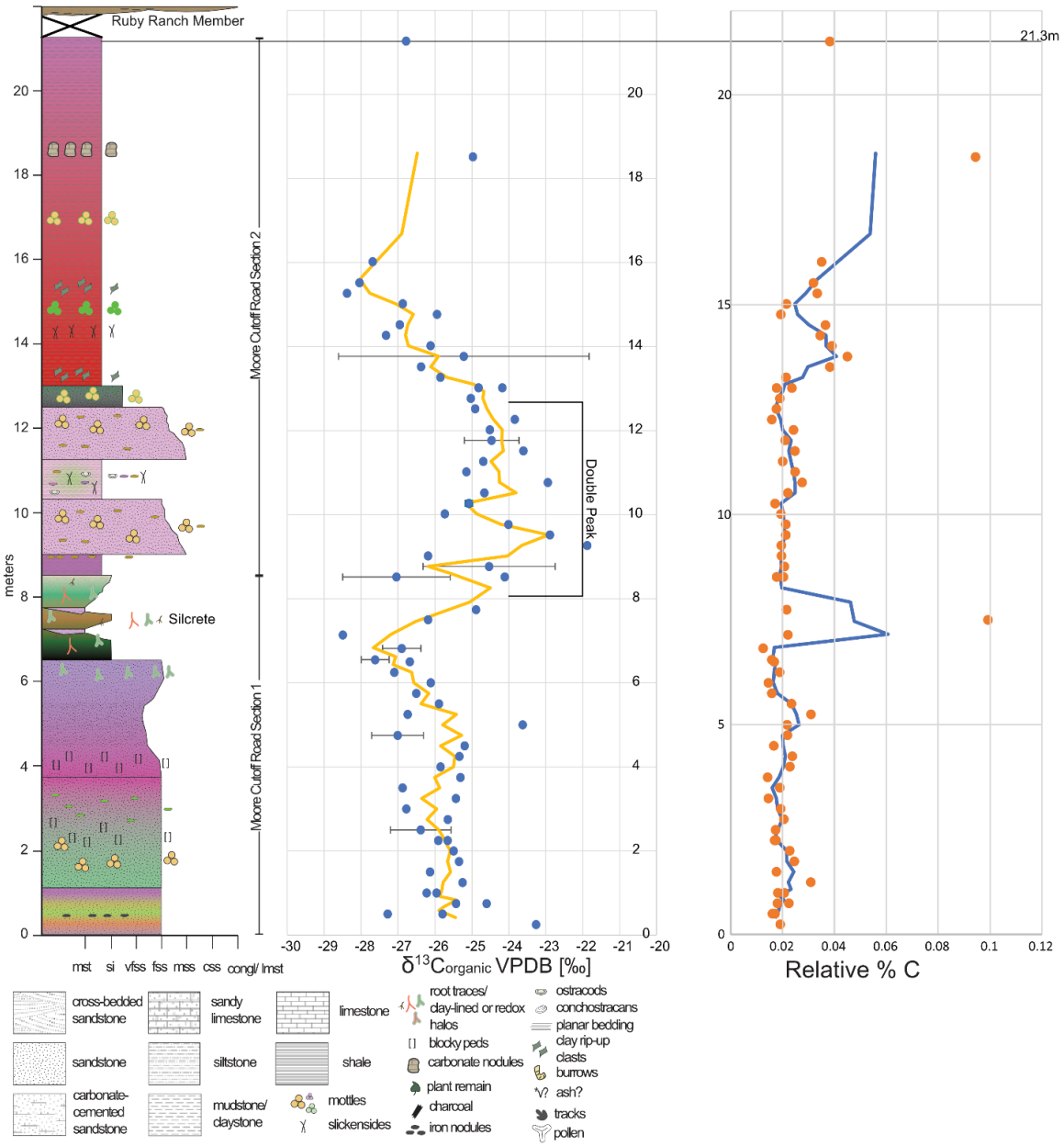

Figure 4: The lithostratigraphy and bulk sedimentary organic carbon stable isotope chemostratigraphy from the Moore Cutoff Road section. Carbon isotope values are compared to VPDB. The solid red line represents the three-point running average of the individual data points represented by the solid blue circles. The silcrete is labelled separately here as the lithostratigraphic labels do not include "silcrete" as such it has been designated siltstone size to differentiate the silica rich layers from the interbedded mudstone layers. The abbreviations in the horizontal scale on the lithostratigraphic column represent the following: mst, mudstone; si, siltstone; vfss, very fine sandstone; fss, fine sandstone; mss, medium sandstone; css, course sandstone; congl/lmst, conglomerate/limestone.

Mussentuchit Member:

The detailed lithostratigraphic description of the Mussentuchit Member section sampled at Moore Cutoff Road can be found in Appendix C. The base of the Mussentuchit is deposited on top of the locally known Short Canyon Member, a hard cliff-forming sandstone/conglomerate (Hunt et al., 2011) within the San Rafael Swell. Based on orthographic photos taken from a drone, its estimated thickness is at ~7.3m and it is deposited on top of the Ruby Ranch Member in this locality. Due to debris and cover, the basal ~2m is covered so the lithological description does not discuss the basal 2m. The uppermost portion of the Short Canyon Member is a tan fine sandstone with abundant charcoal fragments. At ~2m, there is dark gray/black silty mudstones above which lie on fine- to medium-grained sandstones. Above the sandstones are gray silty mudstones with abundant slickensides and root mottles with occasional layers with black carbonized fragments that are inferred to be charcoal. At ~21m, a fine-grained sandstone with bits of charcoal(?) occurs. The primary section measured for the lower portion of the Mussentuchit did not include the uppermost portion so two adjacent sections were collected. The base of the second section, S2, is a gray silty smectic mudstone with slickensides, iron oxide staining, and pieces of charcoal which transitions to a yellow-gray color. The third section, S3, includes some of the yellow gray silty mudstone but towards the uppermost portion transitions to brown and orange sandstones with carbonized fragments as well as abundant leaf fossils.

The values of the $\delta^{13}C_{organic}$ in Figure 5 are from the Mussentuchit Member at the Moore Cutoff Road section. The base of the section is covered by fill for 210cm, so the first samples of the primary section occur ~210cm above the contact with the Short Canyon Member. At the base, the values start at ~-24‰ with a slight trend towards ~-23‰ within the dark, carbon-rich fine sandstones and mudstones. The lithology transitions to dark gray mudstone within which a

moderate PCIE occurs with a magnitude of ~+4‰. The PCIE is maintained for 2.25m between 8.5 and 10.75m but a small NCIE of magnitude -1.5‰ is present within the broader PCIE giving a “double peak” appearance. The lower portion of the PCIE is found within a carbonate-rich sandstone layer. The upper portion is preserved within the more typical dark gray mudstone. A return to pre-excursion values follows with an average ~-25‰. A slight trend towards enriched values occurs reaching a peak at ~-23‰ at 18m before a slight trend back towards more depleted values reaching a minimum of ~-25‰.

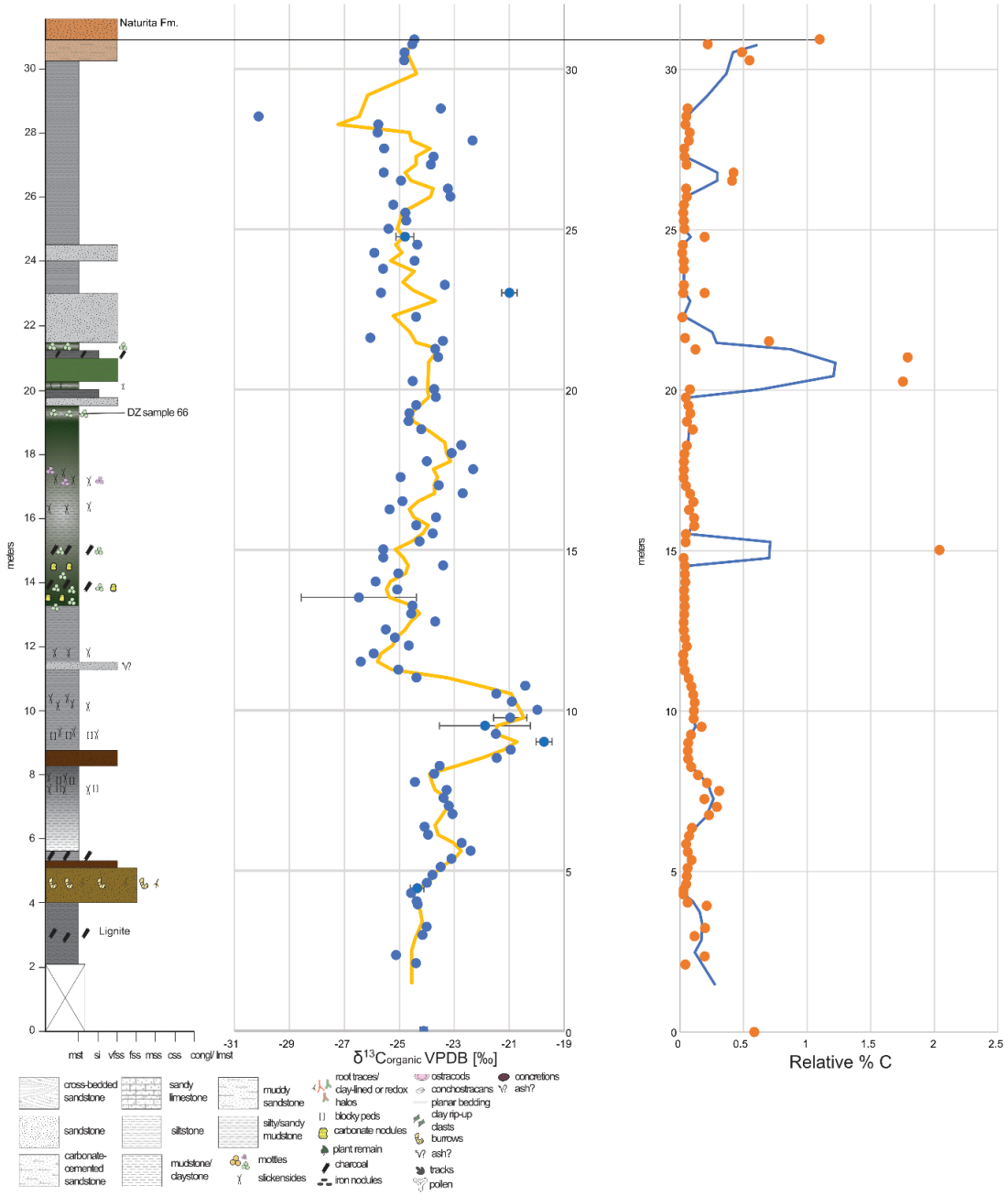

Figure 5: The lithostratigraphy and bulk sedimentary organic-carbon stable isotope chemostratigraphy from the Moore Cutoff Road section for the Mussentuchit Member. Carbon isotope values are compared to VPDB. The yellow line represents the three-point running average of the individual data points represented by the solid blue circles. The lignite within the lower portion of the section is labelled separately and represented by charcoal. The abbreviations in the horizontal scale on the lithostratigraphic column represent the following: mst, mudstone; si, siltstone; vfss, very fine sandstone; fss, fine sandstone; mss, medium sandstone; css, course sandstone; congl/lmst, conglomerate/limestone.

Discussion:

Figure 6 plots all the locations included in this work at their approximate location in a general east-west trend. This figure is mostly applicable for outcroppings of the Yellow Cat Member, but all of the CMF is represented at the Moore Cutoff Road location in the figure with the exception of the Poison Strip Member and Buckhorn Conglomerate. Figure 7 shows the entire CMF chemostratigraphic profile of the Moore Cutoff Road locality plotted against the measured stratigraphic height. Figure 8 represents our interpreted global correlation to sections from Bralower et al., (1999), Herrle et al., (2015), Joo and Sageman, (2014), and Martinez et al., (2015). The Yellow Cat Member is represented by the lower blue curve within the CMF section as is correlated to the astrochronologically-calibrated marine section by Martinez et al., (2015) demonstrating correlation of the carbon cycle perturbation from Weissert Event and the lowermost CMF and Yellow Cat Member. The Mussentuchit Member section is correlated to biostratigraphic and U/Pb geochronology-constrained section from Joo and Sageman (2014) suggesting correlation of the carbon cycle perturbation of the Mid-Cenomanian Event. A comparison of the Yellow Cat Member localities within this work and others is discussed below. This study presents the first published carbon isotope record from the Mussentuchit Member precluding correlation to other Mussentuchit section across the basin, however, additional C-isotope records are forthcoming by our research group.

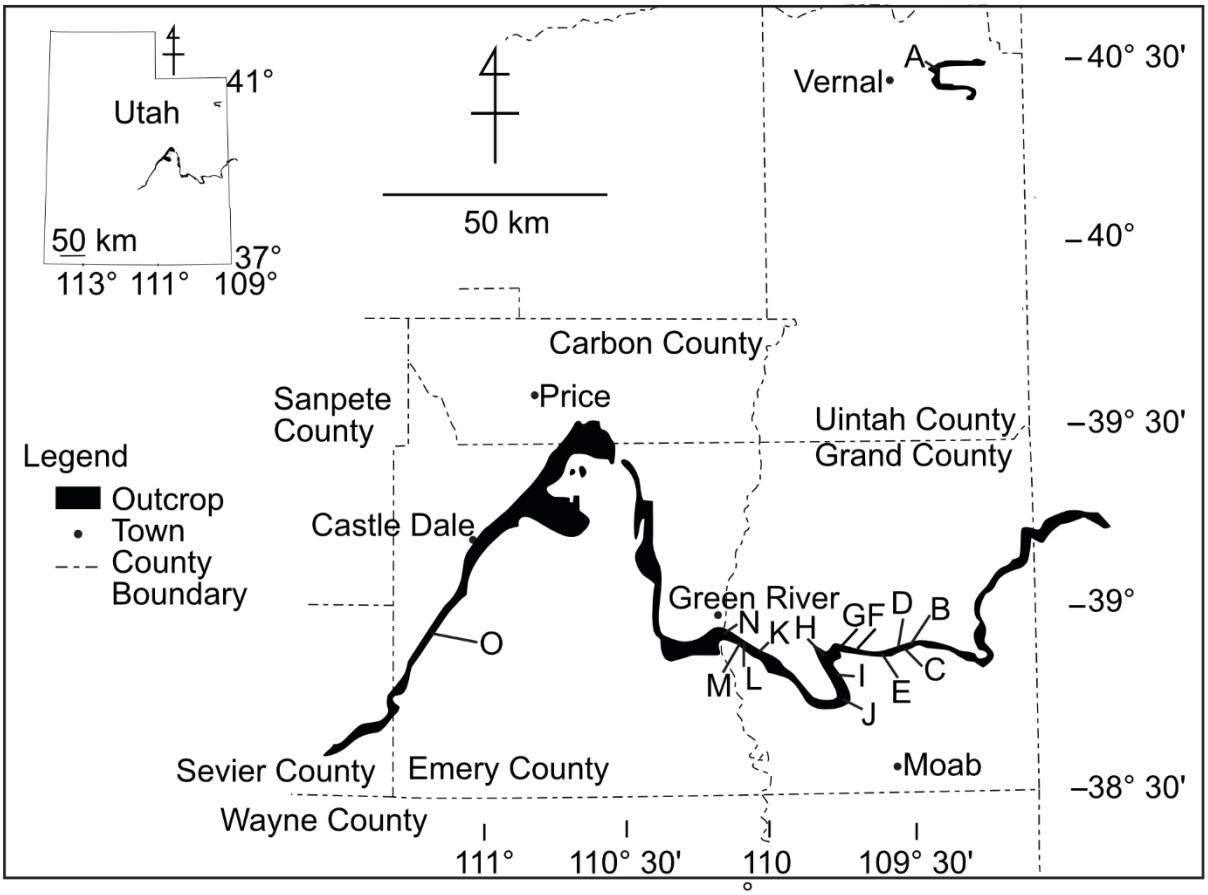

Figure 6 (above): A map of approximate locations of dated Yellow Cat Member localities included in this study. A = Dinosaur National Monument; B = Doelling's Bowl site; C = Near Andrew's site; D = Gaston quarry; E = Yellow Cat Road site; F = Lake Madsen; G = Utahraptor Ridge/Stikes Quarry; H = Jim's Pond; I = Bodily Nodosaur; J = Dalton Wells; K = Ruby Ranch Road; L = Crystal Geyser quarry; M = Suarez Sister's site; N = Don's Ridge; O = Moore Cutoff Road site
Map modified from Mori (2009). Outcrop location as well as localities are from Kirkland and Madsen (2007), Mori (2009), Ludvigson et al. (2010), Kirkland et al. (2016), and Joeckel et al. (2020).

Figure 7 (below): the carbon isotopic ratio as compared to Vienna PeeDee Belemnite plotted against stratigraphic height. The lower portion of data ~20m and lower in blue represent the Yellow Cat Member, the red mid-portion from ~2m up to ~78m represents the Ruby Ranch Member (data is from McColloch (2019) and Gottberg (2022)), and the uppermost section from ~ 85 and up represent the Mussentuchit Member. The gap between the upper Ruby Ranch and lower Mussentuchit is primarily from the Short Canyon Member ~7.3m. The gap between the upper Yellow Cat and lower Ruby Ranch is due to inaccessible rock for sampling ~4.81m.

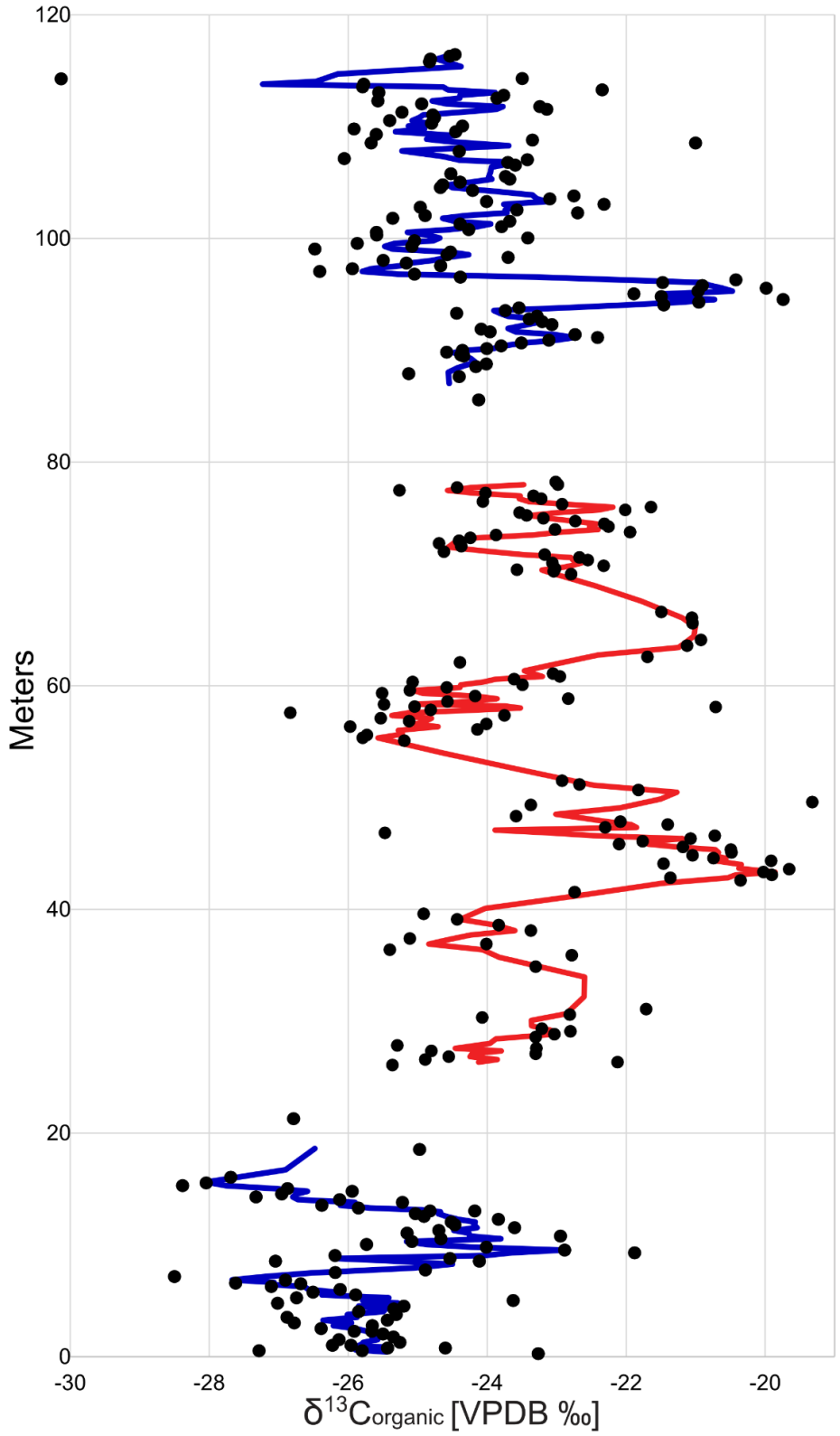
120
100
80
60
40
20
0
Meters
-30
-28
-26
-24
-22
-20
δ13Corganic [VPDB ‰]

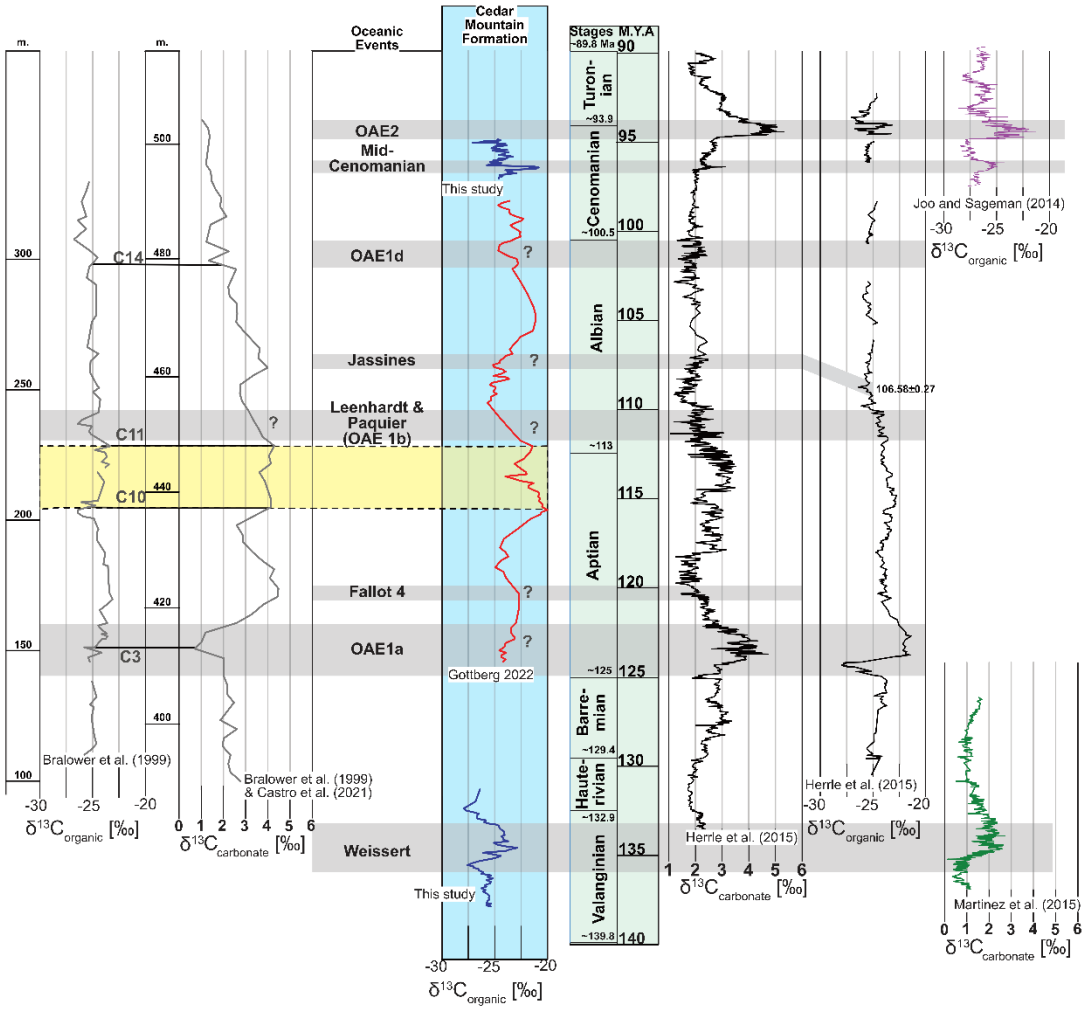

Figure 8: If bounding conditions for the C10 are fixed relative to OAE 1a and OAE 1b in the full CMF chemostratigraphic section to the bounding conditions according to Bralower et al. (1999) and compared to Herrle et al. (2015), Martinez et al. 2015 and Joo and Sageman, 2014. All values are compared to VPDB.

Yellow Cat Member

The Jurassic Morrison Formation provides a lower bound for the age of the CMF at 151.23 ± 3.01 Ma based on $^{40}Ar/^{39}Ar$ age or 151.2 ± 1.8 Ma based on $^{238}U/^{206}Pb$ LA-ICP age of a presumed ashfall bed (Trujillo and Kowallis, 2015). The Yellow Cat Member must be younger than ~151 Ma as it unconformably sits atop the Morrison (Ludvigson et al., 2010; M. B. Suarez et al., 2017). The Yellow Cat Member has been dated using various methods several times in the past two decades in various locations across central and eastern Utah (Greenhalgh, 2006; Britt et al., 2007; Greenhalgh and Britt, 2007; Zeigler, 2008; Mori, 2009; Sames et al., 2010; Ludvigson et al., 2010; Martín-Closas et al., 2013; Hendrix et al., 2015; Kirkland et al., 2016; M. B. Suarez et al., 2017; Joeckel et al., 2020). Early estimates based on detrital zircon U-Pb maximum depositional age gave age of 124 +2/-2.8 Ma (Britt et al., 2007) from Yellow Cat Member sections at Dinosaur National Monument and a maximum depositional age of 124.2 ± 2.6 Ma near Moab, Utah (Greenhalgh, 2006). While the most cited date for the age of the Yellow Cat is a maximum depositional age of 124.2 ± 2.6 Ma from Greenhalgh (2006), it was contradicted by age estimates based on ostracod biostratigraphy four years later (Sames et al., 2010) which put the upper Yellow Cat instead in the Late Berriasian to Valanginian (~142-138 Ma) (Kirkland et al., 2016). The most recent studies on detrital zircon U-Pb dates from the Yellow Cat reinforce this new age range with maximum depositional ages such as 136.3 ± 1.3 Ma found by Joeckel et al., (2020). Also within Joeckel et al. (2020), palynostratigraphic evidence points towards a Berriasian-Hauterivian date for the Yellow Cat Member.

To evaluate the age range of the Yellow Cat Member, a compilation of all the publicly accessible, published (and some unpublished), age estimates for the Yellow Cat Member are found in Appendix D and represents the most complete compilation at present. A large majority

of the sampled sections of the Yellow Cat Member were associated with dinosaur quarries in an attempt to give an age estimates for the bones within. As such, Appendix D is sorted by the location of the dinosaur bone quarries in an approximate east to west trend (Figure 6).

The majority of the detrital radiometric samples from the Yellow Cat Member are from the Barremian or earliest Aptian (following the recent adjustment to the Age/Stage dates found in Gale et al., (2020)) with a slight majority of the samples (eight of 15) between ~119 and ~130 Ma with the remaining samples being older than 135 Ma (Berriasian to Valanginian) with one sample extending back into the mid-Tithonian from the Dalton Wells quarry, likely representing recycled Morrison Formation grains (Greenhalgh, 2006). Only two of the 15 radiometric age estimates fall between ~126 and ~134 Ma (Mori, 2009; Hunt, 2015) giving a somewhat bimodal distribution with the majority of the zircon grains either <~125Ma or >~135 Ma. These 15 radiometric samples only represent nine of the 15 dated sites (with some sites having multiple samples and the remaining 6 sites lacking zircon U-Pb dates) so in order to provide a more complete picture of the age ranges found in the Yellow Cat Member each site will be briefly evaluated here.

The easternmost section is also the northernmost section found within Dinosaur National Monument (Britt et al., 2007). Within Dinosaur National Monument, the Yellow Cat Member is thin (Mori, 2009) with the bulk of the CMF in the area being composed of Ruby Ranch Member and Mussentuchit Member. A detrital zircon analysis conducted by Britt et al. (2007) from the basal portion of the Yellow Cat Member provides a maximum depositional age of 124 +2/-2.8 Ma. Although, this is not an uncommon age for the Yellow Cat Member, there is debate as to whether the naming scheme of the CMF in central Utah can be transferred to this section (Sprinkel et al., 2012).

For the next eastern-most quarry, which is known informally as the Doelling's Bowl quarry and is the type locality for *Yurgovuchia doellingi* (Kirkland et al., 2005a; Senter et al., 2012; Kirkland et al., 2016), a brief study on the zircon provenance for the Yellow Cat Member was conducted by Hunt (2015) who found zircon dates to range between ~130 Ma and 3.323 Ga from a sample within the quarry at the base of the Yellow Cat Member exposure. This single zircon age of ~130 Ma represents one of the two maximum depositional age estimates from the 15 radiometric dates between ~126Ma and ~134 Ma. Another age control from this site is carbon chemostratigraphy. M. B. Suarez et al., (2017) conducted analysis of the chemostratigraphy of the Doelling's Bowl quarry and hypothesized the Yellow Cat Member to be upper Aptian-lower Albian or Valangian-Hauterivian. If correct, M. B. Suarez et al., (2017) would observe the carbon isotope excursion C3 interpreted here as correlative to OAE 1a (Bralower et al., 1999) or the Valanginian Weissert Event excursion (Erba et al., 2004). M. B. Suarez et al., (2017) found the chemostratigraphic profile within Doelling's Bowl to have an oscillatory pattern with no major excursions but attempted to correlate this section with other sections found at their "Lake Madsen", "Near Andrew's Site" and "Yellow Cat Road" sections (discussed later) and found it to be difficult with few correlative portions. With few correlative sections, M. B. Suarez et al., (2017) interpreted the differences in the chemostratigraphic profiles to be a signal that local processes are overriding the signals of global processes but, overall, suggest that the section was too compressed to be evaluated correctly. While no major excursions were observed in the Doelling's Bowl, the lack of excursions is suggestive of a period of stability assuming the chemostratigraphic profile is a primary atmospheric signal. With the addition of the single detrital zircon date of ~130 Ma from Hunt (2015) at the base of the quarry, an another hypothesis can be formed. The lack of excursions suggests the Doelling's Bowl chemostratigraphic profile

represents the relatively stable mid-upper Hauterivian to lowermost Barremian and may instead capture the minor Faraoni Event or the period prior or after and would explain why neither the C3 excursion (and correlated excursion with OAE 1a) nor the Weissert Event excursion were observed within this chemostratigraphic profile. Additional detrital zircon analyses and other methods are recommended for this site.

The next quarry to the west is "Near Andrew's Site". Age constraints are based primarily on a C-isotope chemostratigraphic record also conducted by M. B. Suarez et al., (2017) and is near the dinosaur quarry "Andrew's Site" (the type locality for *Hippodraco*) (Kirkland et al., 2016). Only carbon chemostratigraphy is represented at this location. Similar to the Doelling's Bowl section, this profile was difficult to correlate to their other sections due to the oscillatory pattern with no overall excursions. For this reason, I suggest that the site also represents a stable period between the Weissert Event excursion and C3 (and OAE 1a correlative) excursions. However, with a lack of any other age constraints this interpretation is tenuous and collection of additional age constraints at this site are warranted.

Nearby to "Andrew's Site" is the quarry informally named Gaston Quarry (Kirkland et al., 2016) which is the type locality for *Utahraptor ostrommaysi* (not *Utahraptor ostrommaysorum* which was incorrectly used by Kirkland et al., (2016) as explained by Costa and Normand, (2019)), and *Gastonia burgei* (Kirkland et al., 2016). Few age constraints exist at this quarry as well but a tentative biostratigraphic age of Upper Berriasian to Lowermost Valanginian was concluded based on charophytes (Martín-Closas et al., 2013). This age suggests that *Utahraptor ostrommaysi*, and *Gastonia burgei* and other associated taxa from the quarry are Berriasian – Valanginian age. Additional evidence for an interpretation of Berriasian – Valanginian age is the depositional environment is inferred to be on the shore of a lake

informally known as “Lake Madsen” which, as is described later in this paper, is dated to also be of Berriasian – Valanginian age.

Farther west, a section of samples were taken at the type locality quarry for *Nedcolbertia justinhoffmani,* named informally here as the Yellow Cat Road section, by M. B. Suarez et al., (2017) (see Figure 9) for the construction of a chemostratigraphic profile additional samples were taken by Joeckel et al. (2020) also for use in chemostratigraphic and detrital zircon geochronologic analysis. While M. B. Suarez et al., (2017) had difficulty in correlating their chemostratigraphic profile due to the section being relatively thin, Joeckel et al., (2020) concluded that their chemostratigraphic profile represents a portion of the Weissert Event excursion with a supporting maximum depositional age of 136.3 ± 1.3 Ma from detrital zircons and implies the section from M. B. Suarez et al., (2017) is also a partial section of the Weissert Event excursion. This age constraint on the Yellow Cat Road section along with the new age constraints on the Doelling’s Bowl quarry might explain some of the mismatch between their Yellow Cat Member sections. This adjustment to the age estimates at this quarry implies *Nedcolbertia justinhoffmani* is also of Berriasian – Valanginian age, the same as *Utahraptor ostrommaysi*, and *Gastonia burgei.*

A comparable section to the Yellow Cat Road locality is a locality known informally as “Lake Madsen” due to the lacustrine sediments preserved in the upper portions of the stratigraphic section and deposited within a shallow, likely ephemeral lake due to salt tectonic movement in the Paradox Basin (Sames et al., 2010; Martín-Closas et al., 2013; Kirkland et al., 2016; Joeckel et al., 2020) (see Figure 9). The lake sediments preserve freshwater ostracods which is one of the primary methods with which this section was dated. Sames et al. (2010) estimated this section to be the Late Berriasian to Early Valanginian (~142–138 Ma) based on

these ostracods. The Late Berriasian to Early Valanginian nearly aligns with unpublished palynomorph data from the same site which have been estimated at upper Valanginian to upper Hauterivian (Dr. Carol Hotton, Smithsonian National Museum of Natural History, verbal communications, 2022). A chemostratigraphic section was produced from this locality by Hatzell, (2015) and M. B. Suarez et al., (2017), but unlike the Doelling's Bowl and Near Andrew's Site chemostratigraphic profiles, the Lake Madsen profile has one major NCIE and one major PCIE. If the Yellow Cat Member here is of Berriasian to Hauterivian age as suggested by the palynomorph and ostracod data, then these excursions may represent the excursion associated with the Weissert Event. Additional study using detrital zircons may provide further constraint to the Yellow Cat Member at this locality.

One of the localities with the most radiometric dates is the Utahraptor Ridge/Stikes Quarry (Hendrix et al., 2015; Kirkland et al., 2016; Joeckel et al., 2020) and is the origin of many specimens of *Utahraptor*. Hendrix et al. (2015) dated detrital zircons from the lower, middle, and upper portions of the Yellow Cat Member at this quarry locality and found maximum depositional ages ~136 to ~139 Ma. Ludvigson et al. (in press) also dated detrital zircons from this locality and constructed a chemostratigraphic profile finding a near identical range in detrital zircon ages. They conclude that the section of Yellow Cat Member at this locality is of Berriasian-Valanginian age and may record the Weissert Event excursion as well as some Berriasian carbon isotope excursions that are poorly represented in the literature (see Figure 9).

A locality informally known as "Jim's Pond" (also part of our study) occurs nearby to Utahraptor Ridge/Stikes Quarry. The name is derived from the fact that the deposit is from a shallow, lacustrine environment. This site corresponds to "locality 4" from Joeckel et al., (2020) who, using palynology, suggested a Berriasian-early Hauterivian age for the Yellow Cat Member

at this location. This age is in agreement with the carbon chemostratigraphic profile within this work which suggests a mid-Valanginian-early Hauterivian age based on correlation to the Weissert Event carbon isotope excursion (see Figure 9).

The "Bodily Nodosaur" locality is the site of a polacanthid nodosaur at the base of the top of the undifferentiated Poison Strip/ Yellow Cat section (Mori, 2009). This site was sampled by Mori (2009) for detrital zircon analysis within the Bodily Nodosaur quarry as well as above and below the quarry. The maximum depostional age for the base of the section is at 130 ± 2.4 Ma, within the quarry at 124 ± 2.9 Ma and at the base of the Ruby Ranch Member, above the quarry at 117.2 ± 3.7 Ma. Chemostratigraphy is recommended at this site in order to determine its age relative to other sections.

A heavily excavated locality with an abundant amount of dinosaur bones and taxa is the Dalton Wells quarry west of Moab, Utah (Greenhalgh, 2006; Eberth et al., 2006; Greenhalgh and Britt, 2007; Kirkland et al., 2016; Britt et al., 2017)). This quarry has produced many dinosaur taxa such as *Gastonia bergei, Nedcolbertia justinhoffmani, Utahraptor ostrommaysi, Venenosaurus dicrocei, and Moabosaurus utahensis* (Britt et al., 2017). To approximate the age of the Yellow Cat Member at this locality, other than the abundant dinosaurs, this site was stratigraphically correlated to an eggshell site approximately two kilometers west of BYU's Dalton Wells Quarry (Greenhalgh, 2006; Kirkland et al., 2016) which provided a detrital zircon maximum depositional age of 124.2 ± 2.6 Ma. The quarry itself is 1.5m above the Morrison/Cedar Mountain contact and the secondary locality that provided the ~124 Ma date is 6m above the Morrison/Cedar Mountain contact. This date is the most cited date for the age of the Yellow Cat Member (Kirkland et al., 2016). Within the quarry itself, Greenhalgh, (2006) noted the abundance of likely recycled Jurassic Morrison Formation grains that provided an age

of 146.6 +4.1/-3.9 Ma which is similar to the age of the upper Morrison obtained by Trujillo and Kowallis, (2015). Thus this 146.6 Ma age is thought to predate the age of deposition and instead be an artifact of recycled grains. Greenhalgh (2006) also noted that the quarry sample itself, CM1, did not contain any grains that were of Aptian age like those found at the eggshell site, CM2, nor does it contain a peak in the number of zircons from 166-170 Ma that CM2 does which may in indicative of another source of sediment at CM2 that was not deposited at CM1. They hypothesized that the volcanic event that produced the 124 Ma peak in detrital zircons happened between the deposition of the two samples in the 4.5m stratigraphic difference. This complicates the determination of the age of the Dalton Wells Quarry. As shown above, *Gastonia bergei, Utahraptor ostrommaysi,* and *Nedcolbertia justinhoffmani* are likely Berriasian-Hauterivian. If the Dalton Wells quarry was deposited during the Barremian-Aptian then this implies either a minimum of three taxa, shown above, individually span up to ~19 million years from earliest Berriasian potentially recorded at Utahraptor Ridge/Stikes Quarry (143.1 Ma (Gale et al., 2020; Gomes and Vasconcelos, 2021, Ludvigson et al. (in press))) to ~124 Ma in the Barremian-Aptian. This is unlikely given an estimated median species range for dinosaur species is 7 Ma (Benson, 2018). If the Dalton Wells Quarry is of Berriasian-Hauterivian, this would explain the lack of Aptian grains. The small sample size of 20 youngest analyses chosen from 62 total analyses is also unlikely of capturing Berriasian-Hauterivian grains due to a lull in magmatic activity as noted by Joeckel et al., (2020). In order to resolve this predicament, additional detrital zircon analyses, chemostratigraphic, and/or other biostratigraphic controls are necessary.

A very short exposure of the Yellow Cat Member was measured by Ludvigson et al. (2010), named here as the Ruby Ranch Road locality, below their section of focus in the Ruby

Ranch and Poison Strip Members. They measured carbonate $\delta^{13}C$ from nodular carbonates within the Yellow Cat Member and overlying Poison Strip Member. Within the uppermost Yellow Cat Member, they identified a large PCIE which continues into the lowest Poison Strip before decreasing within the middle Poison Strip. At the peak of the PCIE, which is at the contact between the two members, Ludvigson et al., (2010) measured a U-Pb date from the carbonates. This is the oldest age estimate for the Poison Strip Member and potentially the youngest for the Yellow Cat Member at 119.4 ± 2.6 Ma. The shortness of their chemostratigraphic section and the observation that the date did not originate in the Yellow Cat Member make interpretation of a depositional age difficult for the Yellow Cat Member here. The PCIE in the Yellow Cat Member here could correspond to the Weissert Event if there is a major unconformity between the two or it could correspond to the PCIE associated with OAE 1a. Additional samples from lower in the Yellow Cat Member and a radiometric date from the Yellow Cat Member would provide useful in age determination at this locality.

Two quarries near Crystal Geyser in Grand County, Utah have had detrital zircon samples dated by Mori (2009). These quarries are named Crystal Geyser Quarry after Crystal Geyser itself and the Suarez Sister's site discovered by Dr. Celina Suarez and Dr. Marina Suarez. The Crystal Geyser Quarry is the type locality for *Falcarius utahensis* and has been radiometrically dated using detrital zircons (Kirkland et al., 2005a, b; Mori, 2009). Mori (2009) found dates from samples taken from 50 cm above the quarry, which is 30 cm below a bedded sandstone layer "caprock", and from a paleoriver channel deposit from a hillside 200m from the quarry. The maximum depositional ages they interpreted were 121.8 ± 2.2 Ma and 123.4 ± 4.5 Ma, respectively. These dates provide support for the existence of the Yellow Cat Member in the

uppermost Barremian-lowermost Aptian. This implies *Falcarius utahensis* is likely from the same time period and represents one of the youngest taxa in the Yellow Cat Member.

The second quarry, the Suarez Sister's site located approximately 1 km northwest of the Crystal Geyser quarry, also contains *Falcarius* tentatively linking the sites biostratigraphically. The Suarez Sister's quarry is also the type locality for *Geminiraptor suarezarum* (Senter et al., 2010). Chronostratigraphically, Mori, (2009) dated the Suarez Sister's site by sampling the sandstone immediately above the bone layer and a non-bedded sandstone approximately 1mabove the bone layer. Mori, (2009) had difficulty with the low number of zircons obtained from both samples and opted for a combined analysis of both samples totaling 29 analyses from this site which provided a maximum depositional age of 122.5 ± 2.4 Ma. This matches the Crystal Geyser quarry age and provides an independent age constraint for *Falcarius.*

There is some skepticism of the dates derived by Mori, (2009). Kirkland et al., (2016) questioned the stratigraphic interpretations of Mori (2009) writing "…stratigraphic misinterpretations relative to the stratigraphic framework presented herein and limited sample sizes raise some questions as to the accuracy of those results" (Kirkland et al., 2016, pg. 119). This is in response to samples from above and below the "caprock" providing nearly identical maximum depositional ages. This is in stark contrast to the interpretation that the "caprock" or marker calcrete bed contains a multimillion year hiatus in deposition between the "upper" Yellow Cat Member and "lower" Yellow Cat Member (Aubrey, 1998; Greenhalgh, 2006; Greenhalgh and Britt, 2007; Senter et al., 2010; Kirkland et al., 2016).

Another site nearby called Don's Ridge is the western most locality (Burk, 2014) but is nearby the Crystal Geyser and Suarez Sister's localities (Suarez et al., 2007). Bones from dinosaurs within all three quarries exhibit similar rare earth element (REE) signatures providing

evidence of a similar time period and perhaps shared fauna. While Don's Ridge has provided numerous bones (Kirkland et al., 2016), there has only been one other type of chronostratigraphic dating. Zeigler, (2008) conducted paleomagnetic analyses on the Yellow Cat Member and lower Poison Strip Member. While they had difficulty due to the samples tending to provide poorly defined or incoherent magnetizations, they were able to conclude that the Yellow Cat Member was deposited prior to the Cretaceous Long Normal due to two intervals of reverse polarity in the Yellow Cat and Poison Strip. They tentatively correlate the interval of reverse polarity at the base of the Poison Strip Member to the M0r interval on the geomagnetic time scale defined as occurring from 121.2 ± 0.4 Ma to ~120.7 Ma (Gale et al., 2020; Zhang et al., 2021). This age aligns well with the Crystal Geyser and Suarez Sister's sites providing one more correlation between the sites and additional evidence towards the interpretation by Mori (2009). In addition to the correlation of ages, Suarez et al. (2007) found all of these three sites to have a particular REE signature found in the bones from these quarries. In addition, they not only note the shared REE values in the dinosaur bones between the three aforementioned sites but note the difference between the bones of the three sites and those of the Dalton Wells quarry while all four are of supposed similar ages. A similar study on the REE values in dinosaur bones from the Yellow Cat Member in Dinosaur National Monument should be conducted to conclude whether the REE values are shared between all sites dated at Barremian-Aptian age.

Multiple taxa from Dalton Wells are shared between sites dated as Berriasian-Hauterivian, as shown above, as well as a close similarity of titanosaurs with those of the Upper Saurian beds of the Tendaguru of Tanzania which have been dated to the late Valanginian to Hauterivian (this work; Eberth et al., 2006; Schrank, 2010). It also does not share many taxa with the other Barremian-Aptian age sites in Utah such as *Falcarius* which is shared between Suarez

Sister's site and Crystal Geyser quarry nor does it share REE signatures within the dinosaur bones that the Barremian-Aptian age sites here display. The quarry itself also has not been dated to the Barremian-Aptian with only recycled Jurassic-aged zircons being present. This brings doubt to the age assignment of Dalton Wells to the Barremian-Aptian age. This then implies the existence of at least two "caprocks" or calcrete marker beds. The relative briefness of deposition of the caprock in the Suarez Sister's site and Crystal Geyser quarry implied by the constraining detrital zircon ages found by Mori, (2009) is supported by evidence from the western-most site included here at Moore Cutoff Road.

Across the San Rafael Swell, another exposure of the Yellow Cat Member exists. This site is not included in the Paradox basin as the above sites are and does not include an interval of Poison Strip Member as it is directly overlain by the Ruby Ranch Member. At present only carbon chemostratigraphy has been conducted (this work) and is the first C-isotope record that spans the entire CMF. My interpretation based on the highest resolution C-isotope chemostratigraphic profile to date from the Moore Cutoff Road location and Jim's Pond locality is in agreement with Joeckel et al. (2020). As is shown in Figure 9, the Moore Cutoff Road locality exhibits a large NCIE with subsequent PCIE and 'double peaked' maximum as seen in the Martinez et al. (2015) profile. It is important to note the silcrete section (interpreted here as the "marker" calcrete bed between the "Lower" and "Upper" Yellow Cat Member) towards the middle of the Moore Cutoff Road section is interpreted to be of ~1-2 million year duration at most and not 24 Ma as suggested by other authors (Greenhalgh, 2006; Greenhalgh and Britt, 2007; Kirkland et al., 2016). The Moore Cutoff Road section excursion represents either the Weissert Event excursion or the excursion associated with OAE 1a and is being investigated by our research group through the analysis of detrital zircons, but either interpretation leads to the

conclusion that the marker bed within the Yellow Cat Member at this locality does not represent more than a couple million years at most. It also implies the existence of multiple horizons of calcrete. This implication is supported by existence of a large prominent calcrete found below Stikes Quarry at Utahraptor Ridge which is dated at Berriasian-Valanginian in contrast to the existence of a marker bed "caprock" at the Crystal Geyser and associated sites which are dated as late Barremian-early Aptian (Hendrix et al., 2015; Kirkland et al., 2016; Ludvigson et al., in press). This implication would also explain the supposed incorrect age determination and stratigraphic interpretations levied against Mori (2009) by (Kirkland et al., 2016). Multiple horizons of calcrete also implies multiple episodes of wetting, drying, and calcite formation which is not uncommon for this area as is seen especially in the Ruby Ranch Member (Ludvigson et al., 2010). For future work and further assurance of these conclusions, detrital zircon studies for the Moore Cutoff Road and Jim's Pond localities are necessary to constrain these curves and are forthcoming by our research group.

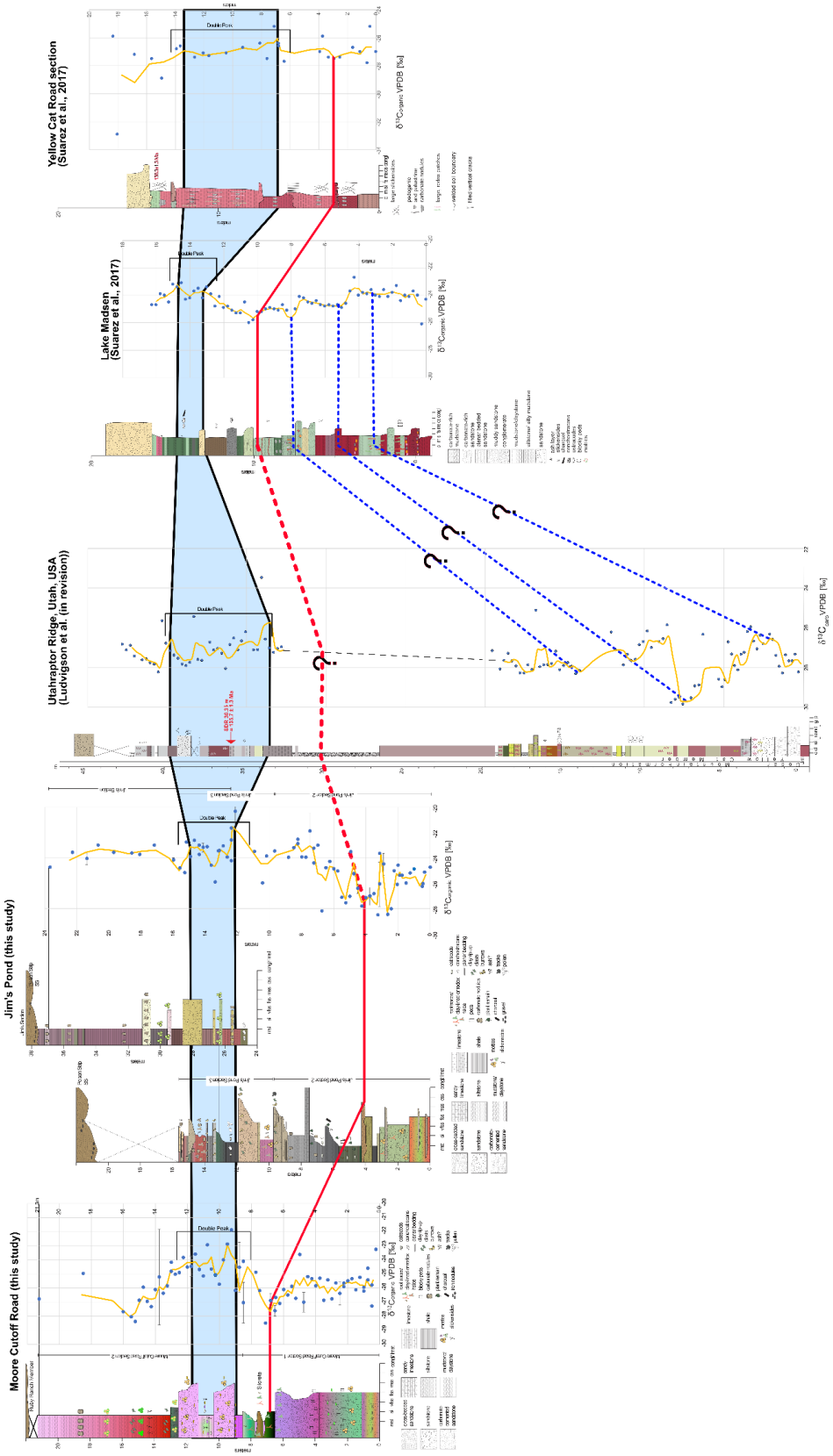

Figure 9: Chemostratigraphic correlation across sites dated to the Berriasian-Late Valanginian. The sections are correlated based on the double peak found in the excursion of the Weissert Event. Some potential correlations are between Utahraptor Ridge, Utah, USA and Lake Madsen. These may represent Berriasian excursions. Stratigraphic columns and chemostratigraphic profiles are modified from Ludvigson et al. (in press) and M. B. Suarez et al. (2017) as well as this work.

Ruby Ranch Member

Work on the Ruby Ranch Member of the CMF is covered further in depth by Ludvigson et al. (2010, 2015), McColloch (2019), and Gottberg (2022) so only a concise review will be included here. A significant amount of work on the Ruby Ranch is presented by Ludvigson et al. (2010) and Ludvigson et al. (2015). A main finding in these two studies is the correlation of the Ruby Ranch C-isotope chemostratigraphic profile as compared with other 'mid' Cretaceous profiles (specifically Erbacher et al., 1996; Bralower et al., 1999; Herrle et al., 2004). Within this work, we agree with this interpretation as represented by the yellow box and dashed lines in Figure 8. In order to add tie points to the Ruby Ranch section with the full Early Cretaceous profile by Herrle et al. (2015), the profile has tie points at the C10 and C11 sections shown in Bralower et al., (1999). Bralower et al. (1999) also identified OAE 1a and OAE 1b within their Santa Rosa Canyon $\delta^{13}C_{organic}$ section along with the C10 and C11 segments (further age constraints is provided by Castro et al., (2021)). OAE 1a and OAE 1b are the tie points between (Bralower et al., (1999) and Herrle et al., (2015). For simplicity, assuming a constant rate of deposition and few major unconformities, our proposal for additional interpretations of the Ruby Ranch section is delineated by question marks in Figure 8. First, the major PCIE associated with the latter half of the Selli Event (OAE 1a) may be preserved in the lowest portion of the Ruby Ranch profile at Moore Cutoff Road. The Fallot 4 event is also shown and may correlate with the coinciding peak in the Ruby Ranch profile. Immediately after the C10 and C11 intervals, signals of OAE 1b is preserved in the Santa Rosa Canyon section by Bralower et al., (1999) and is interpreted to be preserved in the Ruby Ranch section presented by (McColloch, 2019). Additional perturbations from events such as the Jassines and OAE 1d may explain the PCIEs and NCIEs shown in the mid to upper Ruby Ranch particularly OAE 1d as it is composed of four

geologically rapid PCIEs and may correlate to the 3 PCIEs in the upper most Ruby Ranch. U-Pb dates from detrital zircons, carbonates, and volcanic ash bed dates from multiple sections of the Ruby Ranch Member (Ludvigson et al., 2015; and references therein) bracket a broad time scale at their Ruby Ranch Road locality with dates defined between 119 ± 2.6 Ma and 105 ± 4.2 Ma. These age estimates are in line with our interpretation as shown in Figure 8 (with the notable exception of OAE 1a as the chemostratigraphic curve shows a possible OAE 1a excursion but OAE 1a does not fall in between these dates). Additional U-Pb detrital zircon dates from the Moore Cutoff Road section are needed to constrain the carbon-isotope chemostratigraphy.

Mussentuchit Member

Similar to the Ruby Ranch Member, U-Pb geochronology of the Mussentuchit Member at Moore Cutoff Road or Jim's Pond localities have yet to be completed, but has been dated in nearby sections such as Mussentuchit Wash (Tucker et al., 2020) and multiple other sections in Emery County, Utah (e.g. Cifelli et al., 1997), among others. Within the section at Moore Cutoff Road, there is one stratigraphically restricted PCIE. While there are many radioisotope date estimates for the age of the Mussentuchit, there are no other chemostratigraphic profiles for the Mussentuchit Member making this profile the only such profile. As such, at present, we can only compare our chemostratigraphic interpretation against published U-Pb detrital zircon and $^{40}Ar/^{39}Ar$ from volcanic ash beds. The Mussentuchit Member at Moore Cutoff Road is capped by the Naturita Formation. Within Mussentuchit Wash (~30km from Moore Cutoff Road), the lowermost Naturita Formation was interpreted to have a maximum depositional age of 95.64 ± 0.11 Ma (Tucker et al., 2020). We assume the Naturita is a similar age at Moore Cutoff Road which gives an upper bound almost immediately before OAE 2 which spans 94.58 to 93.6 Ma. Vertebrate sites such as 1365-1 within the middle to upper Mussentuchit are dated at 98.37 ±

0.07 Ma (Cifelli et al., 1997) and 99.68 ± 0.12 Ma in Mussentuchit Wash (Tucker et al., 2020). These dates are consistent with the interpretation in Figure 8. Thereby, we tentatively assign the sole PCIE in the Mussentuchit chemostratigraphic curve to be correlative to the Mid-Cenomanian Event (96.4 to 95.8 Ma) rather than OAE 2 which is known to occur within southern outcrops of the Naturita Formation.

The depositional rates for each member of the CMF at Moore Cutoff Road can be roughly estimated based on the dates of portions of the observed carbon isotope excursions. A lack of detrital mineral analyses makes this a preliminary age model but can still be informative of the depositional rates. Figure 10 shows an age model for the CMF at the Moore Cutoff Road locality. This age model helps illustrate the potential unconformity between the Yellow Cat Member and overlying Ruby Ranch Member. The Yellow Cat Member has tie points at the base of the Weissert Event excursion and the first peak within the excursion with astrochronological dates based on 405 ka eccentricity cycles with tie points of CA-ID-TIMS detrital zircon dates from Martinez et al. (2015). The rate between the two points is extrapolated to the lowest and highest samples within the section. The depositional rate is then ~3.7 m/Ma. The Ruby Ranch Member at Moore Cutoff Road has tie points at the C9-C11 excursions bounding the C10 with specific dates based on forminiferal biostratigraphy from Ludvigson et al., (2015) and references therein. The upper and lower portion of the section is then extrapolated from the rate in between the two tie point dates and suggests a depositional rate of ~4.7 m/million years. The Mussentuchit has tie points with the date of the middle of the Mid-Cenomanian Event and the base of OAE 2 from Herrle et al., (2015) and the middle of the Mid-Cenomanian Event from Joo and Sageman, (2014) based on age assignments from references therein. This rate of ~13.7 m/million years is likely an underestimation as it is unlikely that the Mussentuchit ended

deposition at the instant prior to the OAE 2 excursion but even with a conservative estimate the rate is noticeably increased from both the Yellow Cat and Ruby Ranch members.

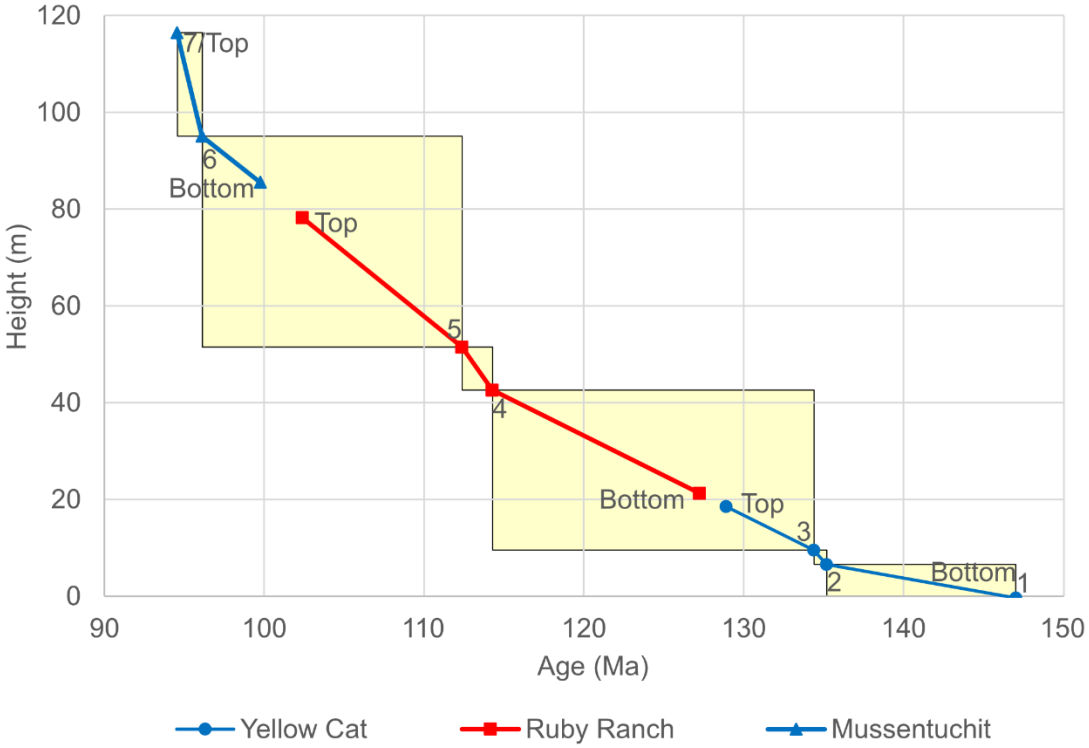

Top and Bottom represent the first sample and last sample of each section. Sampling gaps exist between each member.

1. Top of the Jurassic Morrison (Greenhalgh, 2006)
2. Beginning of Valanginian Excursion
3. First peak of Valanginian Excursion
4. Bottom of C10 Excursion (Ludvigson et al., 2015)
5. Top of C10 Excursion (Ludvigson et al., 2015)
6. Middle of Mid-Cenomanian Event
7. Immediately before OAE 2

Figure 10: Age model for the CMF at Moore Cutoff Road based on data presented in this work as well as Gottberg (2022). The markers for the Yellow Cat Member are the highest and lowest samples within the section as the bounding tie points. The two middle markers represent the beginning of the Valanginian excursion (second marker up from the bottom) and the first peak of the Valanaginian excursion (third marker up from the bottom). For the Ruby Ranch Member, the top and bottom markers represent the top and bottom samples of that section. The two middle points represent the lower and upper bound dates for the C10 excursion of Bralower et al. (1999) extrapolated from the dates of the bounding C9 and C11 excursions with dates from Ludvigson et al. (2015). For the Mussentuchit, the top and bottom markers mark the top and bottom samples of the formation. The middle marker in the Mussentuchit is the location of the Mid-Cenomanian Event. In this curve, the top marker and consequently top sample is placed right before Ocean Anoxic Event 2 so the Mussentuchit curve represents a minimum depositional rate.

Chapter 3: Conclusions

The CMF likely spans the vast majority of the Early Cretaceous and into the earliest Late Cretaceous. This interpretation is not without interruption of deposition or significant erosion. Gaps in deposition likely exist between the Yellow Cat Member/Poison Strip Member and the Ruby Ranch Member. Even with a sampling gap of ~4.81m (covered) between the Yellow Cat Member and the lower Ruby Ranch Member, correlation of the Yellow Cat Member with the C-isotope excursion associated with Weissert Event (Joeckel et al., 2020) suggests a large break in deposition (unconformity) between the Yellow Cat Member and lower Ruby Ranch Member of approximately 10-15 Ma at the Moore Cutoff Road locality and likely between the Yellow Cat Member at the Jim's Pond locality and the Poison Strip Sandstone (Fig. 10). This interpretation is based on interpreted depositional ages of ~131 Ma for the uppermost Yellow Cat Member in these two study sites and the proposed oldest maximum depositional age of the Poison Strip Member (underlying the Ruby Ranch) at ≤ 119 ± 2.6 Ma (Ludvigson et al., 2015). This maximum depositional age may be correlative to the ~10-24 Ma hiatus in deposition observed in some places throughout the Western Cordilleran foreland basin suggesting the deposition of the Yellow Cat Member may be correlative to the initiation and temporary cessation of the Canyon Range thrust in some places (~145-110 Ma) (DeCelles and Coogan, 2006; Hunt et al., 2011; Hunt, 2015; Herring and Greene, 2016) and in others may be due to the influence of salt tectonics (Kirkland et al., 2016; Phillips et al., 2021). It is also proposed that the Yellow Cat and Poison Strip members "were transported in a distal long axial river system with headwaters in the prominent Mogollon Highlands" (Hunt, 2015). A combination of all the above sources and

tectonic drivers can explain the difficulty in correlation of the different Yellow Cat Member sections and chaotically placed depositional locations and stratigraphic relationships.

Based on our current chronostratigraphic framework, we interpret the Ruby Ranch Member to be correlative to latest period of uplift of the Canyon Range Thrust (DeCelles and Coogan, 2006) and was deposited in the foredeep and back-bulge depozones with an east-northeast directed fluvial system providing sediment (Hunt, 2015). The initiation of the Pavant Thrust (western Utah) is then correlative to the deposition of the upper Ruby Ranch Member and Mussentuchit Member. The deposition of the Ruby Ranch and Mussentuchit members may be associated with the relatively slow crustal shortening associated with the Willard thrust at ~125 Ma with an increase in speed at ~105 to 92 Ma (Yonkee et al., 2019; Pujols et al., 2020). The age model agrees with this interpretation given the increase in depositional rate between the Ruby Ranch and Mussentuchit members. Altogether, the CMF includes the majority of the Early Cretaceous and the earliest Late Cretaceous with at least two major unconformities in Yellow Cat Member localities that are assigned a Valanginian-age: one between the Yellow Cat Member and Ruby Ranch/Poison Strip, and one between the Ruby Ranch and Mussentuchit members. In places with Barremian-Aptian age interpretations, the Yellow Cat Member, the Poison Strip Member may interfinger conformably instead of unconformably (Greenhalgh, 2006; Eberth et al., 2006) and would only have one major unconformity between the Ruby Ranch and Mussentuchit members. Overall, our chronostratigraphic framework for Moore Cutoff Road is useful for correlation of other Early Cretaceous deposits within the Western Interior Basin.

Comparable continental formations to the CMF within the Western Interior in nearby states are numerous (ie (DeCelles, 1986; Bonde et al., 2012; Milàn et al., 2015; Ross et al., 2017; Frederickson et al., 2018; D'Emic et al., 2019; Joyce et al., 2020; Di Fiori et al., 2021; Suarez et

al., 2021; Noto et al., 2022; Andrzejewski et al., 2022) and despite this fact, few of these sections have accompanying chemostratigraphic frameworks with the exception of the Wayan Formation and Newark Canyon Formation which have recent initial chemostratigraphic studies (Ross et al., 2017; Todd, 2019).

From a global perspective, the CMF could possibly represent a non-marine, Laurentian North American correlative to the non-marine, Gondwanan African Kem Kem Group, suggesting future chemostratigraphic work be done within the Gara Sbaa and Douira formations of Africa. More specifically, the Mussentuchit Member is comparable in age to the Gara Sbaa and Douira formations (Ibrahim et al., 2020). Analysis of age-equivalent units in Laurentia and Gondwana could provide an opportunity to compare and contrast Early Cretaceous terrestrial environments in opposite hemispheres.

Vertebrate fauna from WIB formations are often correlated to each other. However, based on our interpretations, such correlations should be done with caution especially in quarries where no age constraints exist within the Yellow Cat Member. Kirkland et al., (2016) suggested that a number of faunal turnovers are preserved within the CMF with six overall faunas split between lower Yellow Cat Member, upper Yellow Cat Member, Poison Strip Member, Ruby Ranch Member, and Mussentuchit Member. A Mid-Aptian faunal turnover is hypothesized between the upper Yellow Cat Member and Poison Strip Member but with our new age constraints, a reassessment must be made. Strictly speaking, these turnovers may not necessarily be biotic turnovers, but rather major gaps (up to 24 million years in places, e.g., sites such as the Crystal Geyser quarry, and Suarez Sister's site, where Barremian-Aptian-age Yellow Cat Member is deposited on the late-Jurassic age Morrison Formation) in the vertebrate record. As such, correlation of fauna from the various formations preserved along the Sevier Fold and

Thrust Belt and Western Interior Basin should be done with caution until additional detailed chronostratigraphic work that includes combined U/Pb geochronology, palynology, and C-isotope chemostratigraphy is available for key sections.

Appendix A: Yellow Cat Member at Jim's Pond Locality

Samples* *organized by stratigraphic height	$\delta^{13}C_{organic}$ ‰ vs VPDB	Relative %OC	Cumulative Height	Lithologic Description
JP2-0	-24.80	0.01	0	Section 2 Unit 1: Dark purple fine sandstone with discrete gravel layers fining upward, and green mottling likely reworked from Morrison Formation
JP1-0	-25.18	0.04	35	
JP1-1	-26.09	0.01	45	
JP2-1	-26.30	0.02	50	
JP2-2	-24.93 ± 0.03 3 total analyses	0.02 ± 0.003 3 total analyses	100	
JP2-3	-25.25	0.02	125	
JP2-4	-26.04	0.03	150	Section 2 Unit 2: Gray-green silty/very-fine sandstone with scattered gravel and red/orange mottling Section 2 Unit 3: (sampled for detrital zircon geochron.) Gray medium sandstone
JP2-5	-25.42	0.03	175	
JP1-2	-25.43	0.02	190	
JP2-6	-24.63	0.04	200	
JP1-3	-26.15	0.01	205	
JP2-7	-25.08	0.03	225	
JP1-4	-28.06	0.02	243	
JP2-8	-28.51	1.68	265	
JP2-9	-24.53 ± 0.87 3 total analyses	0.04 ± 0.006 3 total analyses	290	Section 2 Unit 4: Gray-green silty/very-fine sandstone with scattered gravel and red/orange mottling
JP2-10	-23.70	0.07	315	Section 2 Unit 5: Gray-brown silty/very-fine sandstone with scattered gravel
JP1-5	-26.10 ± 1.75 3 total analyses	0.03 ± 0.005 3 total analyses	315	
JP2-11	-28.55	3.70	326	Section 2 Unit 6: Dark gray, organic rich, mudstone
JP2-12	-26.87	0.86	351	

JP2-13	-27.05 ± 0.69 3 total analyses	0.39 ± 0.169 3 total analyses	376	Section 2 Unit 7: Hard grey limestone
JP2-14	-27.19	0.68	401	
JP2-15	-27.85	1.32	426	Section 2 Unit 8 (not sampled): dark thinly laminated mudstone Section 2 Unit 9: Black fissile shale with abundant slickensides and Fe-oxide staining also has abundant ostracods, plant fragments and root traces.
JP2-16	-26.45 ± 0.38 3 total analyses	0.83 ± 0.129 3 total analyses	451	
JP2-17	-25.31	0.33	476	
JP1-6	-23.57	0.02	495	
JP2-18	-27.09	0.37	501	
JP2-19	-27.60	0.45	526	
JP-2-20	-27.17	0.46	551	
JP2-21	-25.09	0.48	576	
JP2-22	-24.92	0.24	601	Section 2 Unit 10: Dark gray finely laminated mudstone that coarsens upward to very fine sandstone includes abundant plant fragments
JP2-23	-24.34	0.29	626	
JP2-24	-24.83	0.13	650	
JP2-25	-28.24	0.40	675	Section 2 Unit 11: Dark gray to medium gray mudstone with ostracods, slickensides, and plant fragments
JP2-26	-23.06	0.13	700	
JP2-27	-24.46	0.07	725	
JP2-27NOD	-23.29	0.35	725	
JP2-28	-21.94 ± 1.46 3 total analyses	0.16 ± 0.018 3 total analyses	750	
JP2-29	-24.01	0.19	775	Section 2 Unit 12: Hard gray limestone
JP2-30	-23.98	0.12	800	Section 2 Unit 13: Dark black, mudstone with
JP2-31	-22.59	0.16	825	
JP2-31NOD	-22.93	0.21	825	

JP2-32	-23.25	0.14	850	slickensides, ostracods, carbonate nodules
JP2-33	-24.01	0.02	883	Section 2 Unit 14: Hard coarse lithic sandstone, planar bedded at base with *Skolithos* at the top
JP2-34	-23.52	0.02	970	
JP3-1	-23.90	0.06	1020	Section 3 Unit 1: Dark red/purple silty mudstone that is finely laminated with Fe-oxide staining, slickensides and root traces with gray green mottling
JP3-2	-26.03	0.07	1045	
JP3-3	-23.55	0.22	1095	Section 3 Unit 2: Quartz sandstone that coarsens upward from fine to medium size, includes *Skolithos* at top
JP3-4	-20.38 ± 1.40 3 total analyses	0.25 ± 0.040 3 total analyses	1215	Section 3 Unit 3: Dark fissile shale with ostracods, slickensides and Fe-oxide staining and rare root traces
JP3-5	-22.64	0.07	1240	
JP-33	-21.71	0.11	1240	
JP-33Burrow	-24.28	0.14	1240	
JP3-6	-24.00	0.07	1265	Section 3 Unit 4: Gray/green clay and mud rich fine-sandstone, interfingers
JP3-7	-23.11	0.04	1290	
JP3-8	-23.48	0.05	1315	
JP-34	-23.51	0.06	1320	

				with Section 3 Unit 3.
JP3-9	-25.95	0.01	1340	Section 3 Unit 5: Light gray, fine grained, massive sandstone
JP3-10	-24.63	0.03	1365	Section 3 Unit 6: Gray/green clay and mud rich fine-sandstone, Section 3 Unit 7: (not sampled) light gray, fine grained, massive sandstone with additional bioturbation
JP3-11	-23.17	0.04	1390	Section 3 Unit 8: Light green-gray siltstone with red/purple carbonate nodules and slickensides
JP3-12	-23.22 ± 0.35 3 total analyses	0.04 ± 0.002 3 total analyses	1415	
JP3-13	-23.78	0.03	1440	Section 3 Unit 9: Fine grained sandstone that coarsens upwards to coarse sized sand with carbonate nodules
JP3-13NOD	-23.06	0.19	1440	
JP3-14	-22.67	0.06	1470	Section 3 Unit 10: Green fine-grained sandstone with carbonate nodules
JP3-15	-23.96	0.06	1495	
JP-35	-22.82	0.08	1520	
JP3-16	-25.21	0.07	1530	Section 3 Unit 11: Interfingering
JP3SEC3TOP	-24.85	0.01	1560	

				fine-grained sandstone and mudstone beds with rare carbonate nodules
JP-36	-24.22 ± 0.21 3 total analyses	0.04 ± 0.002 3 total analyses	1600	Jim's Section Unit 48: Interbedded yellow-gray fine-grained sandstones with silty-sandy calcareous mudstones
JP-37	-23.05	0.04	1720	Jim's Section Unit 49: (not sampled) silty, red, calcareous shale Jim's Section Unit 50: Pale pink very fine calcareous sandstone with root traces
JP-38	-23.78	0.05	1810	Jim's Section Unit 51: Purple-gray mudstone with greenish mottling
JP-39	-23.67	0.05	1860	Jim's Section Unit 52: Pale yellow-gray fine muddy sandstone with concretions
JP-40	-23.62	0.03	1973	Jim's Section Unit 53: Medium to dark red-gray mudstone with concretions
JP-41	-23.05	0.03	2070	
JP-42	-24.10 ± 0.46	0.04 ± 0.003 3 total analyses	2140	Jim's Section Unit 54: Pale

	3 total analyses			green-gray mudstone Jim's Section Unit 55-56: (not sampled) dark gray-green and red mudstones
JP-43	-23.62	0.04	2230	Jim's Section Unit 57: Medium gray-purple sandy mudstone with concretions Jim's Section Unit 58-59: (not sampled) dark green and purple mudstones
JP-44	-24.79	0.03	2370	Jim's Section Unit 60: Pale purple-gray mudstone that coarsens upwards to massive siltstones and very fine sandstones

Appendix B: Yellow Cat Member at Moore Cutoff Road Locality

Samples* *organized by stratigraphic height	$\delta^{13}C_{organic}$ ‰ vs VPDB	Relative %OC	Cumulative Height	Lithologic Description
MCYCM Sec 1-1	-23.26	0.02	25	Unit 1: Dark purple muddy, very fine sandstone with limonite oxide concretions
MCYCM Sec 1-2 Nods	-25.80	0.02	50	
MCYCM Sec 1-2	-27.28	0.02	50	Unit 2: Light purple fine to medium sandstone with yellow mottles and concretions (?)
MCYCM Sec 1-3 nods	-24.60	0.02	75	
MCYCM Sec 1-3	-25.43	0.02	75	
MCYCM Sec 1-4 Nods	-26.22	0.02	100	
MCYCM Sec 1-4	-25.96	0.02	100	
MCYCM Sec 1-5	-25.25	0.03	125	
MCYCM Sec 1-6	-26.13	0.02	150	
MCYCM Sec 1-7	-25.35	0.02	175	
MCYCM Sec 1-8	-25.50	0.02	200	Unit 3: Silty mudstone with floating medium sand grains, ostracods (?), and yellow and green mottles and concretions (Unit fines upward)
MCYCM Sec 1-9 Nods	-25.91	0.02	225	
MCYCM Sec 1-9	-25.66	0.02	225	
MCYCM Sec 1-10	-26.39 ± 0.82 3 total analyses	0.02 ± 0.001 3 total analyses	250	
MCYCM Sec 1-11	-25.65	0.02	275	
MCYCM Sec 1-12	-26.78	0.02	300	Unit 4: light purple, fine-medium sandstone with green and/or yellow mottles and concretions
MCYCM Sec 1-13	-25.43	0.01	325	
MCYCM Sec 1-14	-26.88	0.02	350	
MCYCM Sec 1-15	-25.31	0.01	375	

MCYCM Sec 1-16	-25.85	0.02	400	(Unit fines upward)
MCYCM Sec 1-17	-25.34	0.02	425	Unit 5: dark green, silty, very-fine sandstone mudstone with floating medium sand grains, and yellow and orange mottles and concretions
MCYCM Sec 1-18	-25.20	0.02	450	
MCYCM Sec 1-19	-27.01 ± 0.70 3 total analyses	0.02 ± 0.002 3 total analyses	475	Unit 6: red-purple siltstone with gravel and green rip-up mud clasts Unit 7: (not sampled) Silty, very-fine sandstone with floating medium sand – coarse chert pebbles
MCYCM Sec 1-20	-23.62	0.02	500	
MCYCM Sec 1-21	-26.74	0.03	525	
MCYCM Sec 1-22	-25.89	0.02	550	Unit 8: red-purple siltstone with gravel and green rip-up mud clasts, green mottles, and slickensides (Unit fines upward)
MCYCM Sec 1-23	-26.50	0.02	575	Unit 9: red-purple siltstone with gravel and green rip-up mud clasts and green mottles
MCYCM Sec 1-24	-26.11	0.01	600	
MCYCM Sec 1-25	-27.10	0.02	625	Unit 10: pebble conglomerate green silty

				matrix with green mottles
MCYCM Sec 1-26	-26.68	0.02	650	Unit 11: red-purple siltstone green rip-up mud clasts and green mottles
MCYCM Sec 1-27	-27.62 ± 0.38 3 total analyses	0.02 ± 0.001 3 total analyses	655	
MCYCM Sec 1-28	-26.90 ± 0.52 3 total analyses	0.01 ± 0.001 3 total analyses	682	Unit 12: silty mudstone with floating chert grains (coarse sand sized and pebble sized) with slickensides
MCYCM Sec 1-29	-28.50	0.02	714	
MCYCM Sec 2-33	-26.18	0.10	750	Unit 13: very hard, multicolored silcrete interbedded with red-purple mudstones in the upper portion of the unit includes abundant tree root casts that are silicified but within the red-purple mudstones.
MCYCM Sec 1-30	-24.89	0.02	774	Unit 14: Red-purple silty mudstone interbedded with very fine green-gray sandstones silcretes lower in the unit all with green mottles, some carbonate nodules up section, poorly
MCYCM Sec 1-31	-24.11	0.02	852	
MCYCM Sec 2-1	-27.05 ± 1.46 3 total analyses	0.02 ± 0.001 3 total analyses	852	
MCYCM Sec 2-2	-24.53 ± 1.79 3 total analyses	0.02 ± 0.005 3 total analyses	877	
MCYCM Sec 2-3	-26.19	0.02	902	
MCYCM Sec 2-4	-21.88	0.02	927	

MCYCM Sec 2-5	-22.88	0.02	952	consolidated and highly weathered
MCYCM Sec 2-6	-24.01	0.02	977	
MCYCM Sec 2-7	-25.74	0.02	1002	
MCYCM Sec 2-8	-25.08 ± 0.10 3 total analyses	0.02 ± 0.002 3 total analyses	1027	
MCYCM Sec 2-9	-24.66	0.02	1052	
MCYCM Sec 2-10	-22.94	0.03	1077	
MCYCM Sec 2-11	-25.15	0.02	1102	
MCYCM Sec 2-12	-24.69	0.02	1127	
MCYCM Sec 2-13	-23.60	0.02	1152	
MCYCM Sec 2-14	-24.46 ± 0.74 3 total analyses	0.02 ± 0.005 3 total analyses	1177	
MCYCM Sec 2-15	-24.51	0.02	1202	
MCYCM Sec 2-16	-23.84	0.02	1227	
MCYCM Sec 2-17	-24.91	0.02	1252	
MCYCM Sec 2-18	-25.03	0.02	1277	
MCYCM Sec 2-19	-24.17	0.02	1302	
MCYCM Sec 2-20	-24.82	0.02	1302	*Units are not numbered for the remaining portion of the section* Red-purple siltstone with gravel and green rip-up mud clasts
MCYCM Sec 2-21	-25.85	0.02	1327	
MCYCM Sec 2-22	-26.38	0.04	1352	
MCYCM Sec 2-23	-25.22 ± 3.39 3 total analyses	0.05 ± 0.013 3 total analyses	1377	
MCYCM Sec 2-24	-26.12	0.04	1402	Red-purple siltstone with

MCYCM Sec 2-25	-27.32	0.03	1427	gravel and green rip-up mud clasts, green mottles, and slickensides (Unit fines upward)
MCYCM Sec 2-26	-26.95	0.04	1452	Red-purple siltstone with gravel and green rip-up mud clasts and green mottles
MCYCM Sec 2-27	-25.94	0.02	1477	Pebble conglomerate green silty matrix with green mottles
MCYCM Sec 2-28	-26.87	0.02	1502	Red-purple siltstone green rip-up mud clasts and green mottles
MCYCM Sec 2-29	-28.38	0.03	1527	Silty mudstone with floating chert grains (coarse sand sized and pebble sized) with slickensides
MCYCM Sec 2-30	-28.04	0.03	1552	
MCYCM Sec 2-31	-27.69	0.04	1602	
MCYCM Sec 2-32n	-24.97	0.09	1852	Red-purple silty mudstone interbedded with very fine green-gray sandstones all with green mottles, some carbonate nodules up section, poorly consolidated and highly weathered
MCYCM Sec 2-34	-26.78	0.04	2127	

Appendix C: Mussentuchit Member at Moore Cutoff Road Locality

Sample* *organized by stratigraphic height	$\delta^{13}C_{organic}$ ‰ vs VPDB	Relative % OC	Cumulative Height	Lithologic Description* *Units are not numbered throughout the Mussentuchit
MC-MM-S3-010 top of SCC charcoal site	-24.12 ± 0.13 2 total analyses	0.59 ± 0.190 2 total analyses	0	Fine sandstone with charcoal
MCMM_01	-24.40	0.04	210	Dark gray/black silty mudstone
MCMM_02	-25.12	0.20	235	
MCMM_03	-24.16	0.12	298	
MCMM_04	-24.01	0.20	323	
MCMM_05	-24.34	0.21	393	
MCMM_06	-24.38	0.06	403	Fine-medium greenish-brown sandstone with roots and/or burrowing
MCMM_07	-24.58	0.03	428	
MCMM_08	-24.35 ± 0.25 3 total analyses	0.03 ± 0.009 3 total analyses	443	
MCMM_09	-24.00	0.05	460	
MCMM_10	-23.80	0.05	485	
MCMM_11	-23.50	0.06	510	
MCMM_12	-23.11 ± 2.16 3 total analyses	0.09 ± 0.012 3 total analyses	535	Greyish-brown, muddy, very fine sandstone
MCMM_13	-22.41	0.06	560	Silty mudstone with carbonized pieces of charcoal(?)
MCMM_14	-22.73	0.05	585	Light gray, silty, very fine sandstone with dark grey mottles and slickensides
MCMM_15	-23.96	0.07	610	
MCMM_16	-24.08	0.09	635	
MCMM_17	-23.07	0.23	675	
MCMM_18	-23.21	0.29	700	
MCMM_19	-23.39	0.19	725	
MCMM_20	-23.28	0.31	750	
MCMM_21	-24.44	0.21	775	
MCMM_22	-23.74	0.14	800	
MCMM_23	-23.54	0.09	825	
MCMM_24	-21.46	0.07	850	
MCMM_25	-20.95	0.06	875	
MCMM_26	-19.74 ± 0.29 3 total analyses	0.07 ± 0.003 3 total analyses	900	

MCMM_27	-21.49	0.09	925	
MCMM_28	-21.88 ± 1.65 6 total analyses	0.17 ± 0.070 6 total analyses	950	
MCMM_29	-20.96 ± 0.61 3 total analyses	0.11 ± 0.011 3 total analyses	975	Dark gray mudstone
MCMM_30	-19.98	0.11	1000	Gray silty mudstone
MCMM_31	-20.90	0.12	1025	Light gray silty mudstone with slickensides and root mottles (becomes greenish farther up section with sporadic nodules)
MCMM_32	-21.47	0.10	1050	
MCMM_33	-20.42	0.09	1075	
MCMM_34	-24.38	0.07	1100	
MCMM_35	-25.04	0.04	1125	
MCMM_36	-26.41	0.03	1150	
MCMM_37	-25.94	0.03	1175	
MCMM_38	-24.66	0.05	1200	
MCMM_39	-25.16	0.04	1225	
MCMM_40	-25.49	0.03	1250	
MCMM_41	-23.70	0.03	1275	
MCMM_42	-24.57	0.03	1300	
MCMM_43	-24.53	0.04	1325	
MCMM_44	-26.48 ± 2.09 3 total analyses	0.04 ± 0.019 3 total analyses	1350	
MCMM_45	-25.08	0.03	1375	
MCMM_46	-25.87	0.04	1400	
MCMM_47	-25.04	0.04	1425	
MCMM_48	-23.41	0.04	1450	
MCMM_49	-25.59	0.03	1475	Light gray mudstone with flecks of charcoal (?) and root mottling and slickensides (becomes greenish tinted towards up section)
MCMM_50	-25.59	2.04	1500	
MCMM_51	-24.26	0.05	1525	
MCMM_52	-23.79	0.05	1550	
MCMM_53	-24.39	0.11	1575	
MCMM_54	-23.67	0.11	1600	
MCMM_55	-25.36	0.07	1625	
MCMM_56	-24.89	0.11	1650	
MCMM_57	-22.69	0.08	1675	
MCMM_58	-23.57	0.05	1700	
MCMM_59	-24.96	0.03	1725	
MCMM_60	-22.31	0.03	1750	
MCMM_61	-24.00	0.03	1775	
MCMM_62	-23.10	0.04	1800	
MCMM_63	-22.75	0.06	1825	

MCMM_64	-24.21	0.10	1875	
MCMM_65	-24.67	0.06	1900	
MCMM_66	-24.64	0.08	1925	
MCMM_67	-24.39	0.07	1950	
MCMM_68	-23.67	0.05	1975	Greenish gray very fine sandstone
MCMM_69	-23.73	0.08	2000	Dark gray muddy siltstone with slickensides
MCMM_70	-24.52	1.75	2025	
MCMM_71	-23.59	1.79	2100	Greenish gray very fine sandstone
MCMM_72	-23.70	0.12	2125	Dark gray muddy siltstone with slickensides
MCMM_73	-23.42	0.70	2150	Dark gray muddy siltstone with slickensides and mottles
MCMM_74	-26.05	0.04	2160	Gray-tan fine sandstone with charcoal
MCMM_75	-24.40	0.02	2225	
MCMM_76	-21.00 ± 0.28 3 total analyses	0.19 ± 0.080 3 total analyses	2300	
MC-MM-S2-001	-25.67	0.03	2300	Gray silty smectic mudstone with Fe-oxide staining and slickensides
MC-MM-S2-002	-23.35	0.03	2325	
MC-MM-S2-003	-25.59	0.03	2375	
MC-MM-S2-004	-24.45	0.03	2400	
MC-MM-S2-005	-25.91	0.02	2425	Gray-tan fine sandstone with charcoal
MC-MM-S2-006	-24.35	0.02	2450	
MC-MM-S2-007	-24.80 ± 0.32 3 total analyses	0.19 ± 0.004 3 total analyses	2475	Yellow-gray, sandy-silty, mudstone
MC-MM-S2-008	-25.40	0.04	2500	
MC-MM-S2-009	-24.76	0.03	2525	
MC-MM-S2-010	-24.78	0.03	2550	

MC-MM-S2-011	-25.22	0.03	2575	
MC-MM-S2-012	-23.14	0.05	2600	
MC-MM-S2-013	-23.24	0.05	2625	
MC-MM-S2-014	-24.94	0.41	2650	
MC-MM-S2-015	-25.57	0.42	2675	
MC-MM-S2-016	-23.86	0.05	2700	
MC-MM-S2-017	-23.76	0.04	2725	
MC-MM-S2-018	-25.56	0.03	2750	
MC-MM-S3-001	-22.34	0.07	2775	Gray mudstone with slickensides and Fe-oxide staining
MC-MM-S3-002	-25.79	0.08	2800	
MC-MM-S3-003	-25.77	0.05	2825	
MC-MM-S3-004	-30.13	0.05	2850	
MC-MM-S3-005	-23.49	0.06	2875	
MC-MM-S3-006	-24.83	0.55	3025	Olive gray – orange sandstone with carbon flecks
MC-MM-S3-007	-24.81	0.49	3050	Brown muddy sandstone with carbon flecks
MC-MM-S3-008	-24.53	0.22	3075	Brown muddy sandstone with carbon flecks with abundant leaf fossils
MC-MM-S3-009	-24.46	1.10	3090	Gray shale

Appendix D: Dated Yellow Cat Member Localities

Localities (approx. from East to West)	**Dinosaur National Monument**	**Doelling's Bowl**	**Near Andrew's Site**
Radiometric Dates	124 +2/-2.8 Ma from Detrital Zircons (Britt et al., 2007)	~130Ma from Detrital Zircons (Hunt, 2015 and Kirkland et al., 2016)	None
$\delta^{13}C$ chemostratigraphy	None	Aptian? (M.B. Suarez et al., 2017)	Aptian? (M.B. Suarez et al., 2017)
Ostracod Biostratigraphy	None	None	None
Charophyte Biostratigraphy	None	None	None
Pollen Biostratigraphy	None	None	None
Magnetostratigraphy	None	None	None
Select Dinosaurs		*Yurgovuchia doellingi* (Senter et al., 2012)	

Localities (approx. from East to West)	**Gaston Quarry**	**Yellow Cat Road**	**Lake Madsen**	**Utahraptor Ridge/Stikes Quarry**
Radiometric Dates	None	136.3 ± 1.3 from Detrital Zircons (Joeckel et al., 2020)	None	139.7 ± 2.2; 136.4 ± 1.1; 137.2 ± 2 from Detrital Zircon bottom,

				middle, top of formation (Hendrix et al., 2015 and Joeckel et al., 2020); 135.7 ± 1.3 from Detrital Zircon (Ludvigson et al., in press)
$\delta^{13}C$ chemostratigraphy	None	Valanginian (Joeckel et al., 2020): Aptian? (M.B. Suarez et al., 2017)	Aptian? (M.B. Suarez et al., 2017) Aptian? (Hatzell, 2015)	Berriasian-Valanginian (Ludvigson et al., in press)
Ostracod Biostratigraphy	None		Berriasian-Valanginian (~142-138), (Sames et al., 2010 and Joeckel et al., 2020)	None
Charophyte Biostratigraphy	Upper Berriasian-Lowermost Valanginian from few hundred meters from GQ, (Martin-Closas et al., 2013)		None	None
Pollen Biostratigraphy	None		Upper Valanginian - Upper Hauterivian (Hotton, unpublished)	None
Magnetostratigraphy	None		None	None
Select Dinosaurs	*Utahraptor ostrommaysi, Gastonia burgei* (Kirkland et al., 2005)	*Nedcolbertia justinhoffmani* (Kirkland et al., 1998)		*Utahraptor* (Kirkland et al., 2016)

Localities (approx. from East to West)	**Jim's Pond**	**Bodily Nodosaur**	**Dalton Wells**
Radiometric Dates	None	130 ± 2.9; 124 ± 2.9 from Detrital Zircon below and in bone quarry (Mori, 2009)	146.6 +4.1/-3.9 from Detrital Zircon (likely recycled) D.W. is correlated to nearby

			eggshell site with age of 124.2 ± 2.6 DZ (Greenhalgh, 2006 and Mori, 2009)
$\delta^{13}C$ chemostratigraphy	Valanginian (Forster, this study)	None	None
Ostracod Biostratigraphy	None	None	None
Charophyte Biostratigraphy	None	None	None
Pollen Biostratigraphy	Berriasian-Hauterivian (Joeckel et al., 2020)	None	None
Magnetostratigraphy	None	None	None
Select Dinosaurs		polacanthid nodosaur (Mori, 2009)	*Moabosaurus utahensis, Gastonia bergei, Nedcolbertia justinhoffmani, Utahraptor ostrommaysi, Venenosaurus dicrocei* (Britt et al., 2017)

Localities (approx. from East to West)	**Ruby Ranch Road**	**Crystal Geyser Quarry**	**Suarez Sisters' site**
Radiometric Dates	119.4 ± 2.6 U-Pb in carbonate from Poison Strip Member- Yellow Cat Member contact (Ludvigson et al., 2010)	121.8 ± 2.2 from Detrital Zircon in CGQ, 123.4 ± 4.5 DZ from 200mnorthwest of CGQ (Mori, 2009)	122.5 ± 2.4 DZ from 1 km Northwest of CGQ (Mori, 2009)
$\delta^{13}C$ chemostratigraphy	Aptian? (Ludvigson et al., 2010)	None	None
Ostracod Biostratigraphy	None	None	None
Charophyte Biostratigraphy	None	None	None
Pollen Biostratigraphy	None	None	None
Magnetostratigraphy	None	None	None
Select Dinosaurs		*Falcarius utahensis* (Kirkland et al., 2005)	*Falcarius* (Mori, 2009) *Geminiraptor suarezarum* (Senter et al., 2010)

Localities (approx. from East to West)	**Don's Ridge**	**Moore Cutoff Road**
Radiometric Dates	None	None

$\delta^{13}C$ chemostratigraphy	None	Valanginian (Forster, this study)
Ostracod Biostratigraphy	None	None
Charophyte Biostratigraphy	None	None
Pollen Biostratigraphy		None
Magnetostratigraphy	PSS deposited prior to C34n, Yellow Cat Member maybe shows M0r (Zeigler, 2008)	None
Select Dinosaurs		

References:

Amiot R., Kusuhashi N., Saegusa H., Shibata M., Ikegami N., Shimojima S., Sonoda T., Fourel F., Ikeda T., Lécuyer C., Philippe M. and Wang X. (2021) Paleoclimate and ecology of Cretaceous continental ecosystems of Japan inferred from the stable oxygen and carbon isotope compositions of vertebrate bioapatite. *Journal of Asian Earth Sciences* **205**, 104602.

Amiot R., Wang X., Zhou Z., Wang X., Buffetaut E., Lecuyer C., Ding Z., Fluteau F., Hibino T., Kusuhashi N., Mo J., Suteethorn V., Wang Y., Xu X. and Zhang F. (2011) Oxygen isotopes of East Asian dinosaurs reveal exceptionally cold Early Cretaceous climates. *Proceedings of the National Academy of Sciences* **108**, 5179–5183.

Andrzejewski K., Tabor N., Winkler D. and Myers T. (2022) Atmospheric pCO2 Reconstruction of Early Cretaceous Terrestrial Deposits in Texas and Oklahoma Using Pedogenic Carbonate and Occluded Organic Matter. *Geosciences* **12**, 148.

Arens N. C., Jahren A. H. and Amundson R. (2000) Can C3 plants faithfully record the carbon isotopic composition of atmospheric carbon dioxide? *Paleobiology* **26**, 137–164.

Arthur M. A., Brumsack H.-J., Jenkyns H. C. and Schlanger S. O. (1990) Stratigraphy, Geochemistry, and Paleoceanography of Organic Carbon-Rich Cretaceous Sequences. In *Cretaceous Resources, Events and Rhythms: Background and Plans for Research* (eds. R. N. Ginsburg and B. Beaudoin). NATO ASI Series. Springer Netherlands, Dordrecht. pp. 75–119.

Aubrey W. M. (1998) A newly discovered, widespread fluvial facies and unconformity marking the Upper Jurassic/Lower Cretaceous boundary, Colorado Plateau. *Modern Geology* **22**, 209–233.

Baker S. J., Belcher C. M., Barclay R. S., Hesselbo S. P., Laurin J. and Sageman B. B. (2020) CO2-induced climate forcing on the fire record during the initiation of Cretaceous oceanic anoxic event 2. *GSA Bulletin* **132**, 321–333.

Benson R. B. (2018) Dinosaur macroevolution and macroecology. *Annual Review of Ecology, Evolution, and Systematics* **49**, 379–408.

Bodin S., Godet A., Föllmi K. B., Vermeulen J., Arnaud H., Strasser A., Fiet N. and Adatte T. (2006) The late Hauterivian Faraoni oceanic anoxic event in the western Tethys: Evidence from phosphorus burial rates. *Palaeogeography, Palaeoclimatology, Palaeoecology* **235**, 245–264.

Bodin S., Meissner P., Janssen N. M. M., Steuber T. and Mutterlose J. (2015) Large igneous provinces and organic carbon burial: Controls on global temperature and continental weathering during the Early Cretaceous. *Global and Planetary Change* **133**, 238–253.

Bonde J. W., Varricchio D. J., Bryant G. and Jackson F. D. (2012) Mesozoic vertebrate paleontology of Valley of Fire state park, southern Nevada. In *Field Trip Guide Book for*

the 71st Annual Meeting of The Society Of Vertebrate Paleontology. Carson City: Nevada State Museum pp. 108–126.

Bralower T. J., CoBabe E., Clement B., Sliter W. V., Osburn C. L. and Longoria J. (1999) The record of global change in Mid-Cretaceous (Barremian-Albian) sections from the Sierra Madre, northeastern Mexico. *Journal of Foraminiferal Research* **29**, 418–437.

van Breugel Y., Schouten S., Tsikos H., Erba E., Price G. D. and Sinninghe Damsté J. S. (2007) Synchronous negative carbon isotope shifts in marine and terrestrial biomarkers at the onset of the early Aptian oceanic anoxic event 1a: Evidence for the release of 13C-depleted carbon into the atmosphere. *Paleoceanography* **22**.

Britt B. B., Burton D., Greenhalgh B., Kowallis B., Christiansen E. and Chure D. J. (2007) Detrital zircon ages for the basal Cedar Mountain Formation (Early Cretaceous) near Moab, and Dinosaur National Monument, Utah. In *Geological Society of America Abstracts with Programs* p. 16.

Britt B. B., Scheets R. D., Whiting M. F. and Wilhite D. (2017) Moabosaurus utahensis, n. gen., n. sp., a new sauropod from the Early Cretaceous (Aptian) of North America. *Contributions from the Museum of Paleontology, University of Michigan* **32**, 189–243.

Burk D. (2014) A FOSSIL LOCALITY PREDICTIVE MODEL FOR THE EARLY CRETACEOUS CEDAR MOUNTAIN FORMATION, UTAH, USA. Northwest Missouri State University.

Cao W., Zahirovic S., Flament N., Williams S., Golonka J. and Müller R. D. (2017) Improving global paleogeography since the late Paleozoic using paleobiology. *Biogeosciences* **14**, 5425–5439.

Castro J. M., Ruiz-Ortiz P. A., de Gea G. A., Aguado R., Jarvis I., Weissert H., Molina J. M., Nieto L. M., Pancost R. D., Quijano M. L., Reolid M., Skelton P. W., López-Rodríguez C. and Martínez-Rodríguez R. (2021) High-Resolution C-Isotope, TOC and Biostratigraphic Records of OAE 1a (Aptian) From an Expanded Hemipelagic Cored Succession, Western Tethys: A New Stratigraphic Reference for Global Correlation and Paleoenvironmental Reconstruction. *Paleoceanogr Paleoclimatol* **36**.

Cavalheiro L., Wagner T., Steinig S., Bottini C., Dummann W., Esegbue O., Gambacorta G., Giraldo-Gómez V., Farnsworth A., Flögel S., Hofmann P., Lunt D. J., Rethemeyer J., Torricelli S. and Erba E. (2021) Impact of global cooling on Early Cretaceous high pCO2 world during the Weissert Event. *Nat Commun* **12**, 5411.

Cifelli R. L., Kirkland J. I., Weil A., Deino A. L. and Kowallis B. J. (1997) High-precision 40Ar/39Ar geochronology and the advent of North America's Late Cretaceous terrestrial fauna. *Proceedings of the National Academy of Sciences* **94**, 11163–11167.

Cifelli R. L., Nydam R. L., Gardner J. D., Weil A., Eaton J. G., Kirkland J. I. and Madsen S. K. (1999) MEDIAL CRETACEOUS VERTEBRATES FROM THE CEDAR MOUNTAIN FORMATION, EMERY COUNTY, UTAH: THE MUSSENTUCHIT LOCAL FAUNA.

Utah Geological Survey Miscellaneous Publication **Vertebrate Paleontology in Utah**, 25.

Costa T. V. V. and Normand D. (2019) Commentaries on different uses of the specific epithet of the large dromaeosaurid Utahraptor Kirkland et al., 1993 (Dinosauria, Theropoda). *bzno* **76**, 90–96.

DeCelles P. G. (1986) Sedimentation in a tectonically partitioned, nonmarine foreland basin: The Lower Cretaceous Kootenai Formation, southwestern Montana. *GSA Bulletin* **97**, 911–931.

DeCelles P. G. and Coogan J. C. (2006) Regional structure and kinematic history of the Sevier fold-and-thrust belt, central Utah. *GSA Bulletin* **118**, 841–864.

D'Emic M. D., Foreman B. Z., Jud N. A., Britt B. B., Schmitz M. and Crowley J. L. (2019) Chronostratigraphic Revision of the Cloverly Formation (Lower Cretaceous, Western Interior, USA). *pbmb* **60**, 3–40.

Di Fiori R. V., Long S. P., Fetrow A. C., Snell K. E., Bonde J. W. and Vervoort J. D. (2021) The Role of Shortening in the Sevier Hinterland Within the U.S. Cordilleran Retroarc Thrust System: Insights From the Cretaceous Newark Canyon Formation in Central Nevada. *Tectonics* **40**, e2020TC006331.

Eberth D. A., Britt B. B., Scheetz R., Stadtman K. L. and Brinkman D. B. (2006) Dalton Wells: Geology and significance of debris-flow-hosted dinosaur bonebeds in the Cedar Mountain Formation (Lower Cretaceous) of eastern Utah, USA. *Palaeogeography, Palaeoclimatology, Palaeoecology* **236**, 217–245.

Eldrett J. S., Minisini D. and Bergman S. C. (2014) Decoupling of the carbon cycle during Ocean Anoxic Event 2. *Geology* **42**, 567–570.

Erba E., Bartolini A. and Larson R. L. (2004) Valanginian Weissert oceanic anoxic event. *Geol* **32**, 149.

Erbacher J. and Thurow J. (1997) Influence of oceanic anoxic events on the evolution of mid-Cretaceous radiolaria in the North Atlantic and western Tethys. *Marine Micropaleontology* **30**, 139–158.

Erbacher J., Thurow J. and Littke R. (1996) Evolution patterns of radiolaria and organic matter variations: A new approach to identify sea-level changes in mid-Cretaceous pelagic environments. *Geology* **24**, 499–502.

Föllmi K. B., Bôle M., Jammet N., Froidevaux P., Godet A., Bodin S., Adatte T., Matera V., Fleitmann D. and Spangenberg J. E. (2012) Bridging the Faraoni and Selli oceanic anoxic events: late Hauterivian to early Aptian dysaerobic to anaerobic phases in the Tethys. *Clim. Past* **8**, 171–189.

Frederickson J., Lipka T. and Cifelli R. (2018) Faunal composition and paleoenvironment of the Arundel Clay (Potomac Formation; Early Cretaceous), Maryland, USA. *Palaeontol Electron* **21**, 1–24.

Gale A. S., Bown P., Caron M., Crampton J., Crowhurst S. J., Kennedy W. J., Petrizzo M. R. and Wray D. S. (2011) The uppermost Middle and Upper Albian succession at the Col de Palluel, Hautes-Alpes, France: An integrated study (ammonites, inoceramid bivalves, planktonic foraminifera, nannofossils, geochemistry, stable oxygen and carbon isotopes, cyclostratigraphy). *Cretaceous Research* **32**, 59–130.

Gale A. S., Mutterlose J., Batenburg S., Gradstein F. M., Agterberg F. P., Ogg J. G. and Petrizzo M. R. (2020) The Cretaceous Period. In *Geologic Time Scale 2020* Elsevier. pp. 1023–1086.

Gambacorta G., Jenkyns H. C., Russo F., Tsikos H., Wilson P. A., Faucher G. and Erba E. (2015) Carbon- and oxygen-isotope records of mid-Cretaceous Tethyan pelagic sequences from the Umbria – Marche and Belluno Basins (Italy). *Newsletters on Stratigraphy* **48**, 299–323.

Garrison J. R., Brinkman D., Nichols D. J., Layer P., Burge D. and Thayn D. (2007) A multidisciplinary study of the Lower Cretaceous Cedar Mountain Formation, Mussentuchit Wash, Utah: a determination of the paleoenvironment and paleoecology of the Eolambia caroljonesa dinosaur quarry. *Cretaceous Research* **28**, 461–494.

Gibson S. A., Thompson R. N. and Day J. A. (2006) Timescales and mechanisms of plume–lithosphere interactions: 40Ar/39Ar geochronology and geochemistry of alkaline igneous rocks from the Paraná–Etendeka large igneous province. *Earth and Planetary Science Letters* **251**, 1–17.

Gomes A. S. and Vasconcelos P. M. (2021) Geochronology of the Paraná-Etendeka large igneous province. *Earth-Science Reviews* **220**, 103716.

Gottberg A. (2022) Carbonate Carbon Isotope Chemostratigraphy from the Ruby Ranch Member of the Cedar Mountain Formation in the Western San Rafael Swell. M.S., University of Kansas.

Greenhalgh B. W. (2006) A Stratigraphic and Geochronologic Analysis of the Morrison Formation/Cedar Mountain Formation Boundary, Utah. M.Sc., Brigham Young University.

Greenhalgh B. W. and Britt B. B. (2007) Stratigraphy and Sedimentology of the Morrison–Cedar Mountain Formation Boundary, East-Central Utah. *Central Utah- Diverse Geology of a Dynamic Landscape* **UGA Publication 36**, 81–100.

Gréselle B., Pittet B., Mattioli E., Joachimski M., Barbarin N., Riquier L., Reboulet S. and Pucéat E. (2011) The Valanginian isotope event: A complex suite of palaeoenvironmental perturbations. *Palaeogeography, Palaeoclimatology, Palaeoecology* **306**, 41–57.

Grocke D., Price G., Robinson S., Baraboshkin E., Mutterlose J. and Ruffell A. (2005) The Upper Valanginian (Early Cretaceous) positive carbon–isotope event recorded in terrestrial plants. *Earth and Planetary Science Letters* **240**, 495–509.

Hatzell G. A. (2015) Paleoclimate Implications from Stable Isotope Analysis of Sedimentary Organic Carbon and Vertebrate Fossils from the Cedar Mountain Formation, UT, U.S.A. M.S., University of Arkansas.

Hendrix B., Moeller A., Ludvigson G. A. and Joeckel R. M. (2015) A NEW APPROACH TO DATE PALEOSOLS IN TERRESTRIAL STRATA: A CASE STUDY USING U-PB ZIRCON AGES FOR THE YELLOW CAT MEMBER OF THE CEDAR MOUNTAIN FORMATION OF EASTERN UTAH (2015 GSA Annual Meeting in Baltimore, Maryland, USA (1-4 November 2015)). In *Abstracts with Programs* 7. Geological Society of America, Baltimore, Maryland, USA. p. 597.

Herring D. M. and Greene D. C. (2016) The western Utah thrust belt in the larger context of the Sevier orogeny. *Geological Association Publication* **45**, 131–146.

Herrle J. O., Kößler P., Friedrich O., Erlenkeuser H. and Hemleben C. (2004) High-resolution carbon isotope records of the Aptian to Lower Albian from SE France and the Mazagan Plateau (DSDP Site 545): a stratigraphic tool for paleoceanographic and paleobiologic reconstruction. *Earth and Planetary Science Letters* **218**, 149–161.

Herrle J. O., Schröder-Adams C. J., Davis W., Pugh A. T., Galloway J. M. and Fath J. (2015) Mid-Cretaceous High Arctic stratigraphy, climate, and Oceanic Anoxic Events. *Geology* **43**, 403–406.

Hunt G. J. (2015) U-Pb Detrital Zircon Geochronology of Lower Cretaceous Cedar Mountain and San Pitch Formations in Central-eastern, Utah: A Record of Thrust Belt Unroofing. New Mexico State University.

Hunt G. J., Lawton T. F., Kirkland J. I., Sprinkel D. A., Yonkee W. A. and Chidsey T. C. (2011) Detrital zircon U-Pb geochronological provenance of Lower Cretaceous strata, foreland basin, Utah. *Sevier Thrust Belt: Northern and Central Utah and Adjacent Areas: Utah Geological Association, Publication* **40**, 193–211.

Ibrahim N., Sereno P. C., Varricchio D. J., Martill D. M., Dutheil D. B., Unwin D. M., Baidder L., Larsson H. C. E., Zouhri S. and Kaoukaya A. (2020) Geology and paleontology of the Upper Cretaceous Kem Kem Group of eastern Morocco. *Zookeys* **928**, 1–216.

Jahren A. H., Arens N. C., Sarmiento G., Guerrero J. and Amundson R. (2001) Terrestrial record of methane hydrate dissociation in the Early Cretaceous. *Geol* **29**, 159.

Jarvis I., Gale A. S., Jenkyns H. C. and Pearce M. A. (2006) Secular variation in Late Cretaceous carbon isotopes: a new δ13C carbonate reference curve for the Cenomanian–Campanian (99.6–70.6 Ma). *Geological Magazine* **143**, 561–608.

Joeckel R. M., Ludvigson G. A., Möller A., Hotton C. L., Suarez M. B., Suarez C. A., Sames B., Kirkland J. I. and Hendrix B. (2020) Chronostratigraphy and terrestrial palaeoclimatology of Berriasian–Hauterivian strata of the Cedar Mountain Formation, Utah, USA. *Geological Society, London, Special Publications* **498**, 75–100.

Joo Y. J. and Sageman B. B. (2014) Cenomanian To Campanian Carbon Isotope Chemostratigraphy from the Western Interior Basin, U.S.A. *Journal of Sedimentary Research* **84**, 529–542.

Joyce W. G., Rollot Y. and Cifelli R. L. (2020) A new species of baenid turtle from the Early Cretaceous Lakota Formation of South Dakota. *Fossil Record* **23**, 1–13.

Kirkland J. I., Cifelli R. L., Britt B. B., Park E. D., Burge D. L., DeCourten F. L., Eaton J. G. and Parrish J. M. (1999) Distribution of vertebrate faunas in the Cedar Mountain Formation, east-central Utah. *Utah Geological Survey Miscellaneous Publication* **Vertebrate Paleontology in Utah**, 201–217.

Kirkland J. I., Scheetz R. D. and Foster J. R. (2005a) Jurassic and Lower Cretaceous Dinosaur Quarries of Western Colorado and Eastern Utah. *2005 Rocky Mountain Section of the Geological Society of America Field Trip Guidebook* **402**, 1–26.

Kirkland J. I., Zanno L. E., Sampson S. D., Clark J. M. and DeBlieux D. D. (2005b) A primitive therizinosauroid dinosaur from the Early Cretaceous of Utah. *Nature* **435**, 84–87.

Kirkland J., Suarez M., Suarez C. and Hunt-Foster R. (2016) The Lower Cretaceous in east-central Utah—The Cedar Mountain Formation and its bounding strata. *Geology of the Intermountain West* **3**, 101–228.

Leckie R. M., Bralower T. J. and Cashman R. (2002) Oceanic anoxic events and plankton evolution: Biotic response to tectonic forcing during the mid-Cretaceous: OCEANIC ANOXIC EVENTS AND PLANKTON EVOLUTION. *Paleoceanography* **17**, 13-1-13–29.

Li X., Jenkyns H. C., Wang C., Hu X., Chen X., Wei Y., Huang Y. and Cui J. (2006) Upper Cretaceous carbon- and oxygen-isotope stratigraphy of hemipelagic carbonate facies from southern Tibet, China. *Journal of the Geological Society* **163**, 375–382.

Li X., Wei Y., Li Y. and Zhang C. (2016) Carbon isotope records of the early Albian oceanic anoxic event (OAE) 1b from eastern Tethys (southern Tibet, China). *Cretaceous Research* **62**, 109–121.

Ludvigson G. A., Joeckel R. M., González L. A., Gulbranson E. L., Rasbury E. T., Hunt G. J., Kirkland J. I. and Madsen S. (2010) Correlation of Aptian-Albian Carbon Isotope Excursions in Continental Strata of the Cretaceous Foreland Basin, Eastern Utah, U.S.A. *Journal of Sedimentary Research* **80**, 955–974.

Ludvigson G. A., Joeckel R. M., Murphy L. R., Stockli D. F., González L. A., Suarez C. A., Kirkland J. I. and Al-Suwaidi A. (2015) The emerging terrestrial record of Aptian-Albian global change. *Cretaceous Research* **56**, 1–24.

Martín-Closas C., Sames B. and Schudack M. E. (2013) Charophytes from the Upper Berriasian of the Western Interior Basin of the United States. *Cretaceous Research* **46**, 11–23.

Martinez M., Deconinck J.-F., Pellenard P., Riquier L., Company M., Reboulet S. and Moiroud M. (2015) Astrochronology of the Valanginian–Hauterivian stages (Early Cretaceous): Chronological relationships between the Paraná–Etendeka large igneous province and the Weissert and the Faraoni events. *Global and Planetary Change* **131**, 158–173.

Matthews K. J., Maloney K. T., Zahirovic S., Williams S. E., Seton M. and Müller R. D. (2016) Global plate boundary evolution and kinematics since the late Paleozoic. *Global and Planetary Change* **146**, 226–250.

McColloch C. (2019) Carbon Isotope Chemostratigraphy of the Ruby Ranch Member of the Cedar Mountain Formation Near Moore Cut-Off Road West Central Utah. M.S., The University of Texas at San Antonio.

Merdith A. S., Williams S. E., Collins A. S., Tetley M. G., Mulder J. A., Blades M. L., Young A., Armistead S. E., Cannon J., Zahirovic S. and Müller R. D. (2021) Extending full-plate tectonic models into deep time: Linking the Neoproterozoic and the Phanerozoic. *Earth-Science Reviews* **214**, 103477.

Milàn J., Chiappe L. M., Loope D. B., Kirkland J. I. and Lockley M. G. (2015) First report on dinosaur tracks from the Burro Canyon Formation, San Juan County, Utah, USA : evidence of a diverse, hitherto unknown Lower Cretaceous dinosaur fauna. *Annales Societatis Geologorum Poloniae* **Vol. 85, No. 3**.

Montgomery E. (2014) Limnogeology and chemostratigraphy of carbonates and organic carbon from the Cedar Mountain Formation (CMF), eastern Utah. University of Texas at San Antonio.

Mori H. (2009) Dinosaurian Faunas of the Cedar Mountain Formation and LA-ICP-MS Detrital Zircon Ages for Three Stratigraphic Sections. M.Sc., Brigham Young University.

Neal C. R., Mahoney J. J., Kroenke L. W., Duncan R. A. and Petterson M. G. (1997) The Ontong Java Plateau. In *Geophysical Monograph Series* (eds. J. J. Mahoney and M. F. Coffin). American Geophysical Union, Washington, D. C. pp. 183–216.

Nordt L., Tubbs J. and Dworkin S. (2016) Stable carbon isotope record of terrestrial organic materials for the last 450 Ma yr. *Earth-science reviews* **159**, 103–117.

Noto C. R., D'Amore D. C., Drumheller S. K. and Adams T. L. (2022) A newly recognized theropod assemblage from the Lewisville Formation (Woodbine Group; Cenomanian) and its implications for understanding Late Cretaceous Appalachian terrestrial ecosystems. *PeerJ* **10**, e12782.

Paul C. R. C., Mitchell S. F., Marshall J. D., Leafy P. N., Gale A. S., Duane A. M. and Ditchfield P. W. (1994) Palaeoceanographic events in the Middle Cenomanian of Northwest Europe. *Cretaceous Research* **15**, 707–738.

Phillips S. P., Howell J. A., Hartley A. J. and Chmielewska M. (2021) Coarse-grained meandering distributive fluvial system of the basal Cedar Mountain Formation, USA. *Journal of Sedimentary Research* **91**, 1188–1205.

Pujols E. J., Stockli D. F., Constenius K. N. and Horton B. K. (2020) Thermochronological and Geochronological Constraints on Late Cretaceous Unroofing and Proximal Sedimentation in the Sevier Orogenic Belt, Utah. *Tectonics* **39**.

Raines C. A. (2003) The Calvin cycle revisited. *Photosynthesis research* **75**, 1–10.

Ross J. B., Ludvigson G. A., Möller A., Gonzalez L. A. and Walker J. D. (2017) Stable isotope paleohydrology and chemostratigraphy of the Albian Wayan Formation from the wedge-top depozone, North American Western Interior Basin. *Sci. China Earth Sci.* **60**, 44–57.

Sames B., Cifelli R. L. and Schudack M. E. (2010) The nonmarine Lower Cretaceous of the North American Western Interior foreland basin: New biostratigraphic results from ostracod correlations and early mammals, and their implications for paleontology and geology of the basin—An overview. *Earth-Science Reviews* **101**, 207–224.

Schettino A. and Scotese C. R. (2005) Apparent polar wander paths for the major continents (200 Ma to the present day): a palaeomagnetic reference frame for global plate tectonic reconstructions. *Geophysical Journal International* **163**, 727–759.

Schlanger S. and Jenkyns H. (1976) Cretaceous Oceanic Anoxic Events: Causes and Consequences. *Geologie en Mijnbouw* **55**.

Schrank E. (2010) Pollen and spores from the Tendaguru Beds, Upper Jurassic and Lower Cretaceous of southeast Tanzania: palynostratigraphical and paleoecological implications. *Palynology* **34**, 3–42.

Scotese C. R., Song H., Mills B. J. W. and van der Meer D. G. (2021) Phanerozoic paleotemperatures: The earth's changing climate during the last 540 million years. *Earth-Science Reviews* **215**, 103503.

Scott R. W., Rush N., Hojnacki R., Campbell W., Wang Y. and Lai X. (2020) Albian (Lower Cretaceous) carbon isotope chemozones, Texas Comanche Shelf and Mexican Chihuahua Trough: Implications for OAEs. *Cretaceous Research* **112**, 104453.

Senter P., Kirkland J. I., Bird J. and Bartlett J. A. (2010) A New Troodontid Theropod Dinosaur from the Lower Cretaceous of Utah. *PLOS ONE* **5**, e14329.

Senter P., Kirkland J. I., DeBlieux D. D., Madsen S. and Toth N. (2012) New Dromaeosaurids (Dinosauria: Theropoda) from the Lower Cretaceous of Utah, and the Evolution of the Dromaeosaurid Tail. *PLOS ONE* **7**, e36790.

Seton M., Müller R. D., Zahirovic S., Gaina C., Torsvik T., Shephard G., Talsma A., Gurnis M., Turner M., Maus S. and Chandler M. (2012) Global continental and ocean basin reconstructions since 200Ma. *Earth-Science Reviews* **113**, 212–270.

Sprinkel D. A., Madsen S. K., Kirkland J. I., Waanders G. L. and Hunt G. J. (2012) Cedar Mountain and Dakota formations around Dinosaur National Monument: evidence of the first incursion of the Cretaceous Western Interior Seaway into Utah. *Utah Geological Survey Special Study* **143**, 21.

Suarez C. A., Frederickson J., Cifelli R. L., Pittman J. G., Nydam R. L., Hunt-Foster R. K. and Morgan K. (2021) A new vertebrate fauna from the Lower Cretaceous Holly Creek Formation of the Trinity Group, southwest Arkansas, USA. *PeerJ* **9**, e12242.

Suarez C. A., G. L. MacPherson, David E. Grandstaff, and Luis A. Gonzalez (2007) TAPHONOMIC PUZZLES: USING RARE EARTH ELEMENT GEOCHEMISTRY TO UNRAVEL COMPLEX TAPHONOMY OF VERTEBRATE FOSSIL SITES IN THE YELLOW CAT MEMBER OF THE CEDAR MOUNTAIN FORMATION. In *Geological Society of America Abstracts with Programs,* p. 33.

Suarez C. A., González L. A., Ludvigson G. A., Cifelli R. L. and Tremain E. (2012) Water utilization of the Cretaceous Mussentuchit Member local vertebrate fauna, Cedar Mountain Formation, Utah, USA: Using oxygen isotopic composition of phosphate. *Palaeogeography, Palaeoclimatology, Palaeoecology* **313–314**, 78–92.

Suarez C. A., Gonzalez L. A., Ludvigson G. A., Kirkland J. I., Cifelli R. L. and Kohn M. J. (2014) Multi-Taxa Isotopic Investigation of Paleohydrology In the Lower Cretaceous Cedar Mountain Formation, Eastern Utah, U.S.A.: Deciphering Effects Of the Nevadaplano Plateau On Regional Climate. *Journal of Sedimentary Research* **84**, 975–987.

Suarez C., Knobbe T., Crowley J., Kirkland J. and Milner A. (2017) A chronostratigraphic assessment of the Moenave Formation, USA using C-isotope chemostratigraphy and detrital zircon geochronology: Implications for the terrestrial end Triassic extinction. *Earth and Planetary Science Letters* **475**, 83–93.

Suarez M. B., Ludvigson G. A., González L. A., Al-Suwaidi A. H. and You H.-L. (2013) Stable isotope chemostratigraphy in lacustrine strata of the Xiagou Formation, Gansu Province, NW China. *Geological Society, London, Special Publications* **382**, 143–155.

Suarez M. B., Suarez C. A., Al-Suwaidi A. H., Hatzell G., Kirkland J. I., Salazar-Verdin J., Ludvigson G. A. and Joeckel R. M. (2017) Terrestrial Carbon Isotope Chemostratigraphy in the Yellow Cat Member of the Cedar Mountain Formation: Complications and Pitfalls eds. K. E. Zeigler and W. G. Parker. *Terrestrial Depositional Systems*, 303–336.

Tejada M. L. G., Suzuki K., Kuroda J., Coccioni R., Mahoney J. J., Ohkouchi N., Sakamoto T. and Tatsumi Y. (2009) Ontong Java Plateau eruption as a trigger for the early Aptian oceanic anoxic event. *Geology* **37**, 855–858.

Todd A. (2019) Sedimentology and Chemostratigraphy of the Devil's Gate Section of the Newark Canyon Formation. M.S., University of Colorado at Boulder.

Trabucho-Alexandre J. T., Van Gilst R. I., Rodríguez-López J. P. and De Boer P. L. (2011) The sedimentary expression of oceanic anoxic event 1b in the North Atlantic: OAE 1b in the North Atlantic. *Sedimentology* **58**, 1217–1246.

Trujillo K. C. and Kowallis B. J. (2015) Recalibrated Legacy 40Ar/39Ar Ages for the Upper Jurassic Morrison Formation, Western Interior, U.S.A. *Geology of the Intermountain West* **2**, 1–8.

Tucker R. T., Zanno L. E., Huang H.-Q. and Makovicky P. J. (2020) A refined temporal framework for newly discovered fossil assemblages of the upper Cedar Mountain Formation (Mussentuchit Member), Mussentuchit Wash, Central Utah. *Cretaceous Research* **110**, 104384.

Weissert H. and Erba E. (2004) Volcanism, CO_2 and palaeoclimate: a Late Jurassic–Early Cretaceous carbon and oxygen isotope record. *Journal of the Geological Society* **161**, 695–702.

White W. M. (2014) *Isotope Geochemistry*., John Wiley & Sons.

Yonkee W. A., Eleogram B., Wells M. L., Stockli D. F., Kelley S. and Barber D. E. (2019) Fault Slip and Exhumation History of the Willard Thrust Sheet, Sevier Fold-Thrust Belt, Utah: Relations to Wedge Propagation, Hinterland Uplift, and Foreland Basin Sedimentation. *Tectonics* **38**, 2850–2893.

Zanno L. E. and Makovicky P. J. (2013) Neovenatorid theropods are apex predators in the Late Cretaceous of North America. *Nat Commun* **4**, 2827.

Zeigler K. E. (2008) Stratigraphy, paleomagnetism and magnetostratigraphy of the Upper Triassic Chinle Group, north-central New Mexico and preliminary magnetostratigraphy of the Lower Cretaceous Cedar Mountain Formation, eastern Utah. Ph.D., The University of New Mexico.

Zhang Y., Ogg J. G., Minguez D., Hounslow M. W., Olaussen S., Gradstein F. M. and Esmeray-Senlet S. (2021) Magnetostratigraphy of U-Pb–dated boreholes in Svalbard, Norway, implies that magnetochron M0r (a proposed Barremian-Aptian boundary marker) begins at 121.2 ± 0.4 Ma. *Geology* **49**, 733–737.